55
56

Corrosion Resistance of Modified ß-Eucryptite

by

Laurent P. Battu

Thesis submited to the Faculty of the

Virginia Polytechnic Institute and State University

in partial fulfillment of the requirements for the degree of

Master of Science

in

Materials Engineering

APPROVED:

Dr. Jesse J. Brown Jr., Chairman

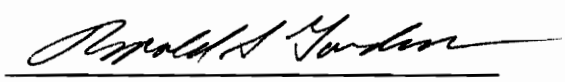

Dr. Ronald S. Gordon, Department Head

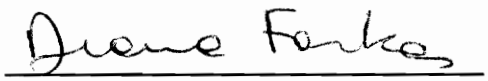

Dr. Diana Farkas

April 1991

Blacksburg, Virginia

CORROSION RESISTANCE OF MODIFIED ß-EUCRYPTITE

by

Laurent Pierre Battu

Jesse J. Brown, Chairman

Materials Engineering

(ABSTRACT)

The corrosion resistance of chemically modified ß-eucryptite ($Li_{0.41}Mg_{0.035}AlP_{0.52}Si_{0.48}O_4$) having low expansion anisotropy and a near zero coefficient of thermal expansion was evaluated. Samples were exposed to aqueous hydrochloride acid at temperatures up to 100°C and environments containing sodium sulfate up to 1000°C. The corrosion resistance was characterized by dilatometry, scanning electron microscopy, X-ray diffraction, energy dispersive x-ray analysis, weight variations, and mechanical properties variations.

The results show that modified ß-eucryptite is more severely corroded than commercial lithium-alumina-silicate glass-ceramics when exposed to these environments. Aqueous HCl removes $AlPO_4$ from modified ß-eucryptite leaving a very porous structure. Molten salt corrodes modified ß-eucryptite by penetration of sodium and sulfur which form an alkali melt under the surface. The modulus of rupture and the Young's modulus are reduced by both types of corrosion.

ACKNOWLEDGEMENTS

I wish to express my gratitude for the constant support and guidance given by my advisor, Dr. Jesse J. Brown, during my studies. I am deeply grateful for the privilege he gave me of working on this research project with the Center for Advanced Ceramic Materials. I also wish to express my thanks to Dr. Diana Farkas and Dr. Ronald S. Gordon for serving on my committee.

I also would like to give special thanks to Dr. Deidre Hirschfeld for her assistance and support during this research and her editorial assistance. I also wish to thanks Nancy Brown for her editorial assistance.

I would like to thanks Mrs. Ruth Hallman, Mr. Bob Hallman, Ms Holly Lesko, and Mrs. Suzan Fleming for their constant assistance and support during this project.

I would like to give a special thanks to my office mates Kyoung-Ho Lee and James Liu for their support, advice, and friendship through the last two years. They made me laugh and enjoy my stay in this lab. I would like to thank also all of my fellow graduate

students within the center, Jeanie, Sandra, Diane, Steve, Yaping, Taiwei, Bob, Eric, and Karen for their support and friendship. They will all be missed, but hold a special place in my heart.

I would like to thank my roommates, Brett, Wojteck, and Takemi and all my friends Benoit, Jeffy, Anne, Antonio, Sylvaine and Jean Christophe "Choubes", Christophe, Bertrand, Rodolphe, Dolly, Andrei, Bruno and Eva, Lisa, Pascale and Cathy, Yves and Catherine, Marc, Hervé, Jean-Yves and Sylvie, "GI Jef", Fred, Remi and Marie, Thierry, Marten, Linda and Bob who made me enjoy my stay at Virginia Tech.

Finally I would like to thank my girlfriend, Véronique, my sister, Isabelle, and my parents and grandparents for their love, encouragements, patience, understanding and support through all of these years.

TABLE OF CONTENTS

LIST OF FIGURES

LIST OF TABLES

CHAPTER 1. INTRODUCTION

The cost of petroleum together with environmental concerns are responsible for the development of advanced more efficient internal combustion engines. To be significantly more efficient, engines have to operate at high temperatures. To fulfill this goal, ceramics, such as silicon carbide, silicon nitride, NZP and LAS glass-ceramics, have been developed for thermal barrier applications and high temperature structural applications in these advanced engines. With higher operating temperatures, the effects of corrosion are enhanced. Impurities in fuels such as sulfur products can react with sodium chloride ingested with the air to form sodium sulfate, and deposit on the surface of the ceramic in the form of molten salt film. These deposits can lead to severe corrosion, with a destruction of the surface and a diminution of the mechanical properties.

ß-eucryptite, a lithium-aluminum-silicate (LAS) glass-ceramic which has negative bulk thermal expansion, is being investigated for use in heat engine applications. During chemical attack, ions exchanges occur between the glass-ceramic and the environment. This leads to an increase in the tensile stresses at the grain boundaries and microcracking[1]. It is believed that the large expansion anisotropy between the a and c axes of ß-eucryptite amplifies the formation of microcracks thus augments its poor corrosion resistance to acid

and molten salts. A chemically modified ß-eucryptite which exhibits reduced anisotropy and near zero thermal expansion coefficient was recently developed at Virginia Tech. This research evaluates the corrosion resistance of $AlPO_4$ modified ß-eucryptite and compares it with commercial LAS. Samples were corroded by aqueous hydrochloride acid at temperatures up to 100°C, and to environments containing sodium sulfate at temperatures up to 1000°C. The corrosion resistance was characterized by dilatometry, scanning electron microscopy (SEM), X-ray diffractometry (XRD), energy dispersive X-ray analysis (EDX), variations in weight loss, and variations in mechanical properties.

CHAPTER 2. LITERATURE REVIEW

2.1 Glass-ceramics

The interest in ceramic materials has increased greatly in the past twenty years because their applications have been extended to many new fields, such as the automotive, the aerospace, and other industries where there is exposure to high temperatures. Glass-ceramic materials have been available for a long time, and many new applications have been developed in the past few years such as the ones described by Vogel[2], Paul[3], and Strinad[4] which include machinable glass-ceramics, high-strength glass ceramics, solder glass ceramics, bioglass-ceramics, and low thermal expansion glass-ceramics. Glass-ceramics are made using conventional glass-forming processes. Once the glass is formed, it is then heat treated to produce a dense polycrystalline ceramic (Figure 2.1).

In glass-ceramic processing, nucleation and crystal growth are very important steps. A nucleating agent is usually added such as TiO_2, ZrO_2, or P_2O_5 which controls the nucleation, and also assures a fine-grain microstructure.

The most important glass-ceramic compositions are members of the following systems.

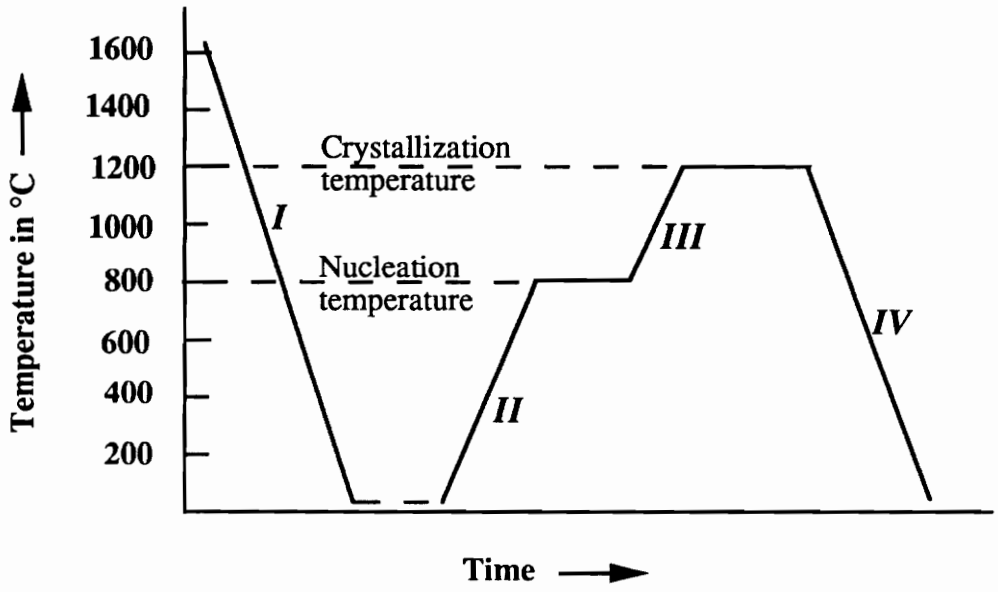

Figure 2.1: Schematic of the formation of a glass-ceramic as a function of time and temperature in stages I to IV (Vogel, Ref. 2)

I Glass processing
II Nucleation
III Crystallization
IV Annealing of final product

-Li_2O-Al_2O_3-SiO_2 (LAS): Glass-ceramics having very low thermal expansion coefficient such as ß-eucryptite and ß-spodumene are of this type.

-MgO-Al_2O_3-SiO_2 (MAS): These are interesting because they form machinable glass-ceramics, and because of their electrical characteristics.

-Li_2O-ZnO-SiO_2: These are noted for their high mechanical strength.

The properties of these materials can vary greatly in a controlled manner depending on the chemical composition of the glass and on the heat treatment used. They have relatively small dimensional changes during the phase transformation from glass to glass-ceramic. If there are no bubbles in the melt, a glass-ceramic can be pore-free. Usually, porosity does not develop during the conversion from the glass to the ceramic state because the overall volume change is very small (3% compared to values up to 50% during drying and firing of conventional ceramics). The densities of glass ceramics are approximately the same as those of conventional ceramics. Generally, if the glass phase present after heat treatment is small, the glass-ceramics have good chemical stability and corrosion resistance.

One advantage of the glass-ceramics is the variety of thermal expansion coefficients that can be obtained; ranging from high which are a good match with metals, to very low or even negative as found in the LAS system in which important thermal shocks resistance can be obtained. This is a very important factor in high temperature applications where thermal shock may cause microcracks which would result in the deterioration of the mechanical properties.

Glass-ceramics are known for their good mechanical properties, particularly strength and toughness. For example, Pyroceram 9606 V, a LAS glass-ceramic, maintains a bending strength of 203 MPa[2] up to 1000°C. Glass-ceramics materials often possess higher Young's moduli than other conventional ceramics[2]. The toughness of glass-

ceramics is enhanced because the two phase structure inhibits cracks growth. These mechanical properties have made the glass-ceramics very attractive in high temperature applications such as structural parts in engines[2,3]. Their low thermal expansion coefficient make them even more attractive in these applications because they have good resistance to thermal shock.

However, one problem encountered in some glass-ceramics is their thermal expansion anisotropy. Thermal expansion anisotropy leads to a reduction of mechanical properties because of microcracking and decrease corrosion resistance[1].

2.2 Modified ß-eucryptite

Kingery[5] described the Li_2O-Al_2O_3-SiO_2 system (LAS) as one of the most important commercial glass-ceramic system because of its very high resistance to thermal shock. The following two compositions are of particular interest:

-ß-spodumene, Li_2O-Al_2O_3-$4SiO_2$, which possesses a small positive thermal expansion coefficient[1] ($9x10^{-7}$/°C).

-and ß-eucryptite, Li_2O-Al_2O_3-$2SiO_2$, which has a negative thermal expansion ($-70x10^{-7}$/°C).

One problem encountered with ß-eucryptite is the high thermal expansion anisotropy between the a-axis and the c-axis. The CTE value along the a-axis is $81.1x10^{-7}$/°C and along the c-axis is $-169x10^{-7}$/°C which gives an overall negative bulk thermal expansion coefficient[6].

Fucinari[1] proposed that this large expansion anisotropy was responsible for the high susceptibility of ß-eucryptite to chemical attack. During the corrosion process, he proposed

an ion exchange mechanism. The large anisotropy results in large intergranular stresses which increase when the ion exchange occurs. Those stresses at the grain boundaries lead to microcracking.

In order to reduce this anisotropy and improve corrosion resistance, a chemically modified ß-eucryptite has been developed by Yang and Brown[7]. A solid solution was obtained between $AlPO_4$ and ß-eucryptite which has the high quartz structure. The following composition, $Li_{0.41}Mg_{0.035}AlP_{0.52}Si_{0.48}O_4$, has a near zero thermal expansion (-2.3×10^{-7}/°C compared to the -70×10^{-7}/°C for pure ß-eucryptite), and a drastically reduced anisotropy (Figure 2.2). To improve the high temperature stability of ß-eucryptite 20 mol% of Li^+ is remplaced by Mg^{2+} because Li^+ is unstable at elevated temperatures. This substitution also decreases the thermal expansion anisotropy. It is this composition, referred to as modified ß-eucryptite, that has been chosen for this research.

2.3 Corrosion

2.3.1 Background

There are three basic corrosion reactions in ceramic materials as classified by Richardson[8] and by Lay[9]. They are gas-solid reactions such as oxidation, liquid-solid reactions such as corrosion by an aqueous solution, and solid-solid reactions where the ceramic reacts with the material which supports it. These different reactions can occur at various temperatures, from room temperature to 1200°C in some heat engine applications, and up to even higher temperatures when the ceramic is used as a lining in the manufac-

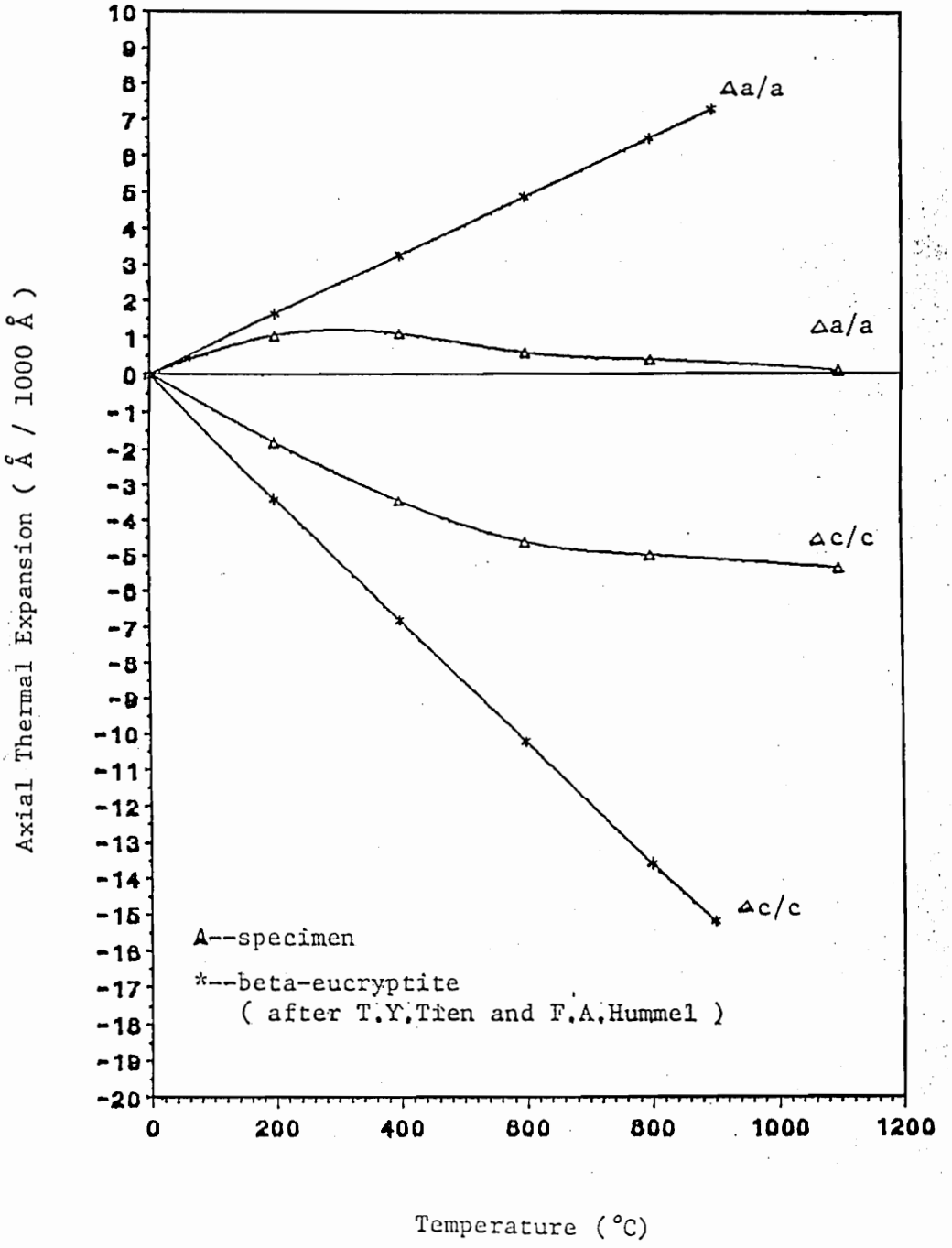

Figure 2.2: Axial thermal expansion (Yang and Brown Ref. 7) for ß-eucryptite (*) and for modified ß-eucryptite (Δ)

turing of metals or glasses. The mechanisms[10] which these reactions occurs include dissolution, reduction, hydration, and oxidation.

Depending on the kinetics and on the nature of the product reaction, the corrosion can either be passive or active. Passive corrosion occurs when the corrosion products form a protective layer at the surface. For example, in the case of oxidation of silicon carbide or silicon nitride, a silica layer is formed on the surface at elevated temperature and high oxygen partial pressure. This protective layer controls the oxidation by controlling the oxygen diffusion through the SiO_2 layer.

Active corrosion takes place when no protective layer is formed on the surface of a corroded ceramic, there is active corrosion. Again, in silicon carbide and silicon nitride, this is the case when oxygen partial pressure is lower than 1 mm Hg according to Richerson[8]. Silicon monoxide gas forms which will not protect the ceramic.

Blacher and Pettit[11] have pointed out that the major role of impurities on the corrosion behavior of alumina, silica, and silicon based ceramics, particularly at high temperature (1000°C) is the promotion of the corrosion reactions at the grain boundaries. The grain boundaries facilitate diffusion of gases and corrosion products and thus increase the corrosion rate.

An application of considerable interest for LAS materials, and especially modified ß-eucryptite, is in hostile environments of gas turbine engines or advanced heat engines. NaCl present in the intake air or other sodium impurities present in the fuel can combine at

high temperatures with sulfur impurities also present in the fuel. Fox et al.[12] proposed the following reaction:

$$2\ NaCl(s) + SO_3(g) + H_2O(g) = Na_2SO_4(l) + 2\ HCl(g)$$

This reaction indicates that corrosion by both HCl and molten salts Na_2SO_4 should be investigated.

2.3.2 HCl Corrosion

Sato et al.[13] described the corrosion of silicon nitride by aqueous HCl solutions. In this work, hot-pressed Si_3N_4 containing Y_2O_3, Al_2O_3, and AlN were corroded in pH 1 and pH -1 HCl aqueous solution at 50°C to 1000°C. The Y^{3+} and Al^{3+} ions present in the grain boundary phase were dissolved by HCl. Si^{4+} present in the matrix was not dissolved. The degree of dissolution was determined from data obtained from atomic absorption spectrometry, and showed that the corrosion was controlled by a surface-chemical reaction for low HCl concentrations, or by diffusion for high HCl concentration. However, the overall corrosion was very limited. A linear decrease in the fracture strength (three point bending) with increasing degree of dissolution of Y^{3+} and Al^{3+} ions was observed.

Because Si_3N_4 is also a prime candidate for heat engine applications, some work has been done by Marra[14] and MacNallan[15] on high temperature (950°C) corrosion by HCl. They have shown that the corrosion is very limited due to the SiO_2 layer on the

sample surface. Here again the corrosion was largely influenced by the presence of additive and impurities such as Fe, Al_2O_3, B, C, Y_2O_3.

There is only limited information on the corrosion of LAS materials. Fucinari[1] studied corrosion of LAS materials exposed to sulfuric acid. He described the corrosion as an ion exchange where the lithium ions interacted with hydrogen ions. Because hydrogen ions are smaller in size, this produced a contraction of the basic structure and a decrease of the thermal expansion, even when the material was exposed to dilute solutions. Then, after repeated exposure, microcracks formed and a increase in the thermal expansion was observed (Figure 2.3). This microcracking was attributed to the increase in tensile stresses at the grain boundaries due to the contraction of the individual crystallites.

2.3.3 Na_2SO_4 Corrosion

In gas turbine engines, ingested sodium chloride can react with sulfur impurities from the fuel to form sodium sulfate. This sodium sulfate can deposit on engine parts as a molten salt (melting temperature: 884°C) and lead to severe corrosion. Many papers have been published by Jacobson, Smialek and Fox[12,16-20] on the molten salts corrosion of silicon carbide and silicon nitride at high temperatures. In order to reproduce the gas turbine engine conditions, the samples were coated by a thin salt layer by airbrushing a saturated solution on the samples (a salt layer of 2 to 3 mg/cm2). The samples were preheated at 200°C and then placed in a horizontal furnace at 1000°C under various gas mixtures such as air, SO_3-SO_2, and oxygen atmospheres. Small partial pressures of SO_2 and SO_3

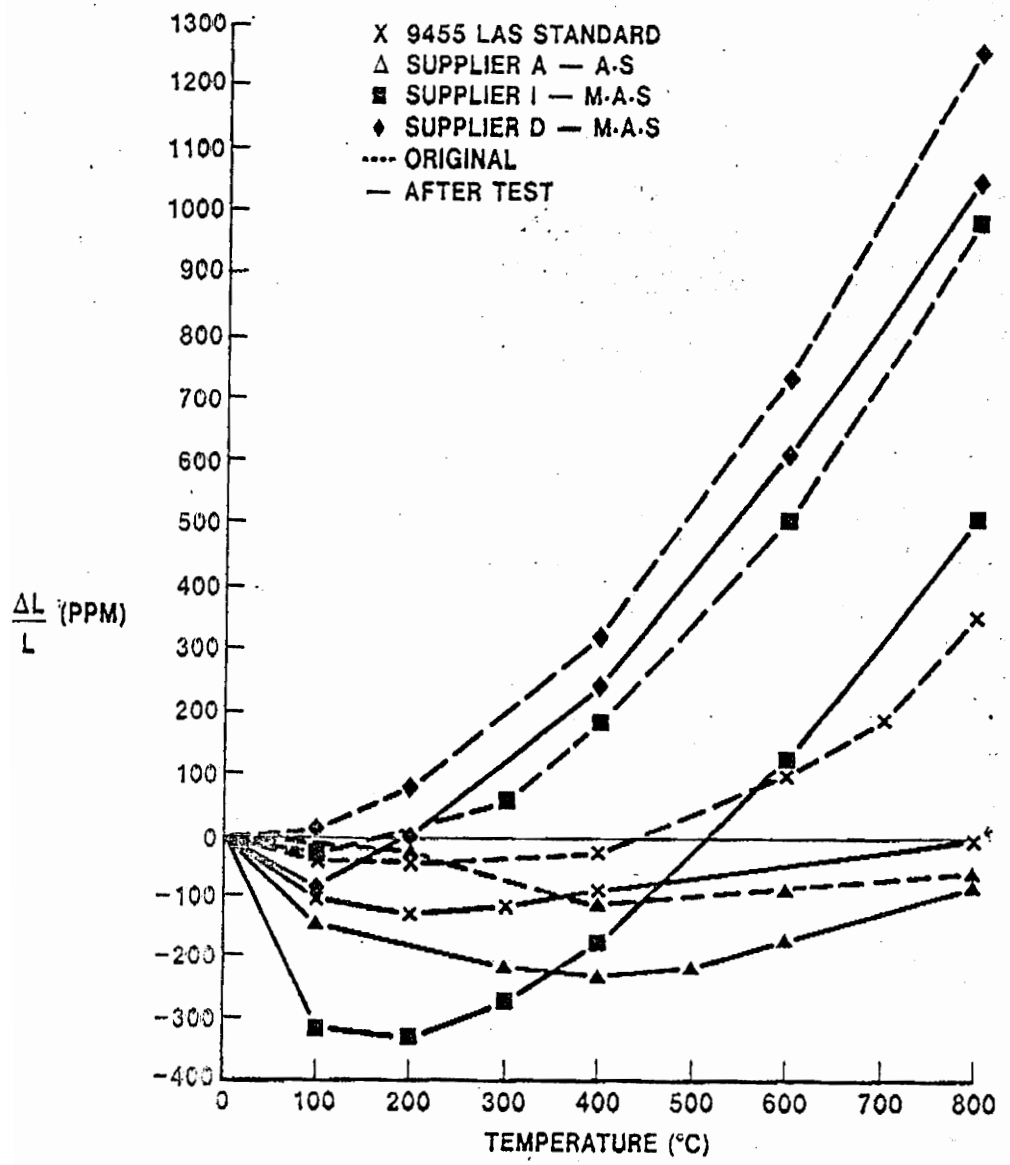

Figure 2.3: Matrix thermal expansion before and after exposure to sulphuric acid simulating cold face regenerator test conditions (Ref. 1)

(P_{SO_2}=100Pa and P_{SO_3}=10Pa) were used to lower the Na_2O activity in accordance with the following reactions:

$$Na_2SO_4(l) = Na_2O(s) + SO_3(g) \qquad a_{Na_2O}=K1/P_{SO_3}$$

and

$$Na_2SO_4(l) = Na_2O + SO_2(g) + 1/2O_2$$

$$a_{Na_2O}=K_2/(P_{SO_2}P_{O_2})$$

When in presence of air only, sodium sulfate decomposed entirely and gave an high sodium oxide activity. The corrosion formed a smooth glassy product layer which caused uneven pitting and grain boundary attack. This layer was primarily SiO_2 and $Na_2 \cdot x(SiO_2)$. The weight gains were in the same order of magnitude when in the atmosphere, SO_2 and SO_3 was injected at very low partial pressure (10 and 100 Pa respectively). Similar results were obtained with Na_2CO_3/CO_2 corrosion.

In all cases, the reaction caused a dramatic etching of the SiC substrate. The attack occurred by dissolution of the protective oxide film. This rapidly formed film was reported to enhance the gas permeability.

Bianco[21] investigated the corrosion of cordierite ($2MgO \cdot 2Al_2O_3 \cdot 5SiO_2$) by sodium sulfate at 1000°C. In this case oxidation was not part of the process as it was in the case of silicon carbide and silicon nitride because cordierite is already an oxide. Both burner rig corrosion and thin salt film attack were studied. In the case of the thin salt attack, the samples were coated by 2.5 mg/cm^2 of salt. They were exposed to air, oxygen, and 1%

SO_2 - O_2 atmospheres at a temperature of 1000°C. After only 1 hour of corrosion by a thin salt layer, $NaAlSiO_4$ was detected. After 8 hours of corrosion, Na_2SO_4 had completely decomposed and the sodium had reacted to form part of the corrosion scale. Formation of Mg_2SiO_4 in the surface layer was also reported in some cases. Two hypotheses were given for this formation: (1) a devitrification of the glassy grain boundary phase in the cordierite enhanced by sodium, leading to a new phase and with a volume change or (2) Na_2SO_4 penetration into cordierite and creation of cracks upon cooling[21].

In the burner rig tests, the samples were placed above a flame of commercial fuel with injected salt. Similar results than with the thin salt film attack were observed.

Van Der Biest[22] reported the role that sulfur might play in the high temperature corrosion of ceramics in petrochemical applications. Sulfur participated in the removal of SiO_2 by formation of SiS via SiO. The following mechanism was particularly important at high sulfur-low oxygen environments:

$$SiO_2(s) + 1/2S_2(g) = SiO(g) + 1/2O_2(g) + 1/2S_2(g) = SiS(g) + O_2(g)$$

Fucinary[1] examined corrosion by sodium on LAS materials. Here, the ion exchange between lithium and sodium caused the structure to expand, increasing the bulk volume of the matrix as well as the bulk thermal expansion. Samples were soaked in 3.5% sodium chloride solution, dried and then fired at 800°C. The extent of the reaction was then observed by measuring the dimensional changes and the bulk thermal expansion (Figure 2.4). Standard Corning 9455 LAS gave the smallest dimensional changes compared to other glass-ceramics.These dimentional changes were attributed to microcraking type of dammage.

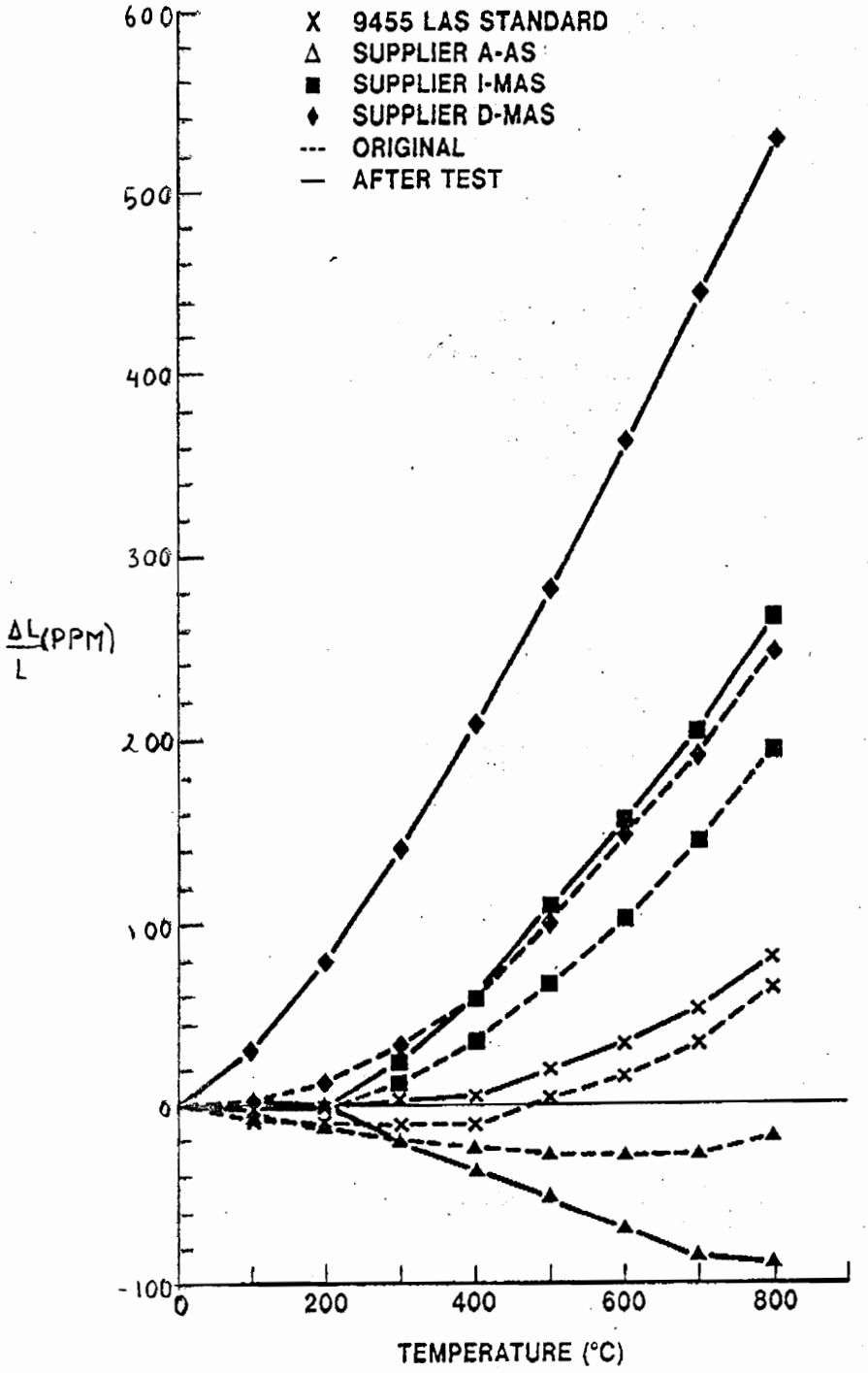

Figure 2.4: Thermal expansion before and after exposure to sodium simulating hot face regenerator test conditions (Ref. 1)

A very important aspect of ceramics is their mechanical properties at high temperature as discussed previously. These mechanical properties are also affected by corrosion. Fox[12] and Smialek[18] reported strength reduction when SiC was exposed to high temperature corrosion, and found pitting in SiC and grain boundary attack in Si_3N_4. This led to reduction of room temperature flexural strength (Figure 2.5). Molten salt corrosion was reported to degrade more of the mechanical properties, such as flexural strength and fracture toughness, than simple oxidation. Similar findings were also reported by Kim and Moorhead[23] where the changes in flexural strength were not significant when passive oxidation occurred, but a 50% reduction of strength was observed when active oxidation occurred. Cao[24] found that the amorphous deposits, which were formed during high temperature oxidation or corrosion, resulted in strength limiting flaws and continuous microstructural changes that affected both the creep rate and fracture toughness.

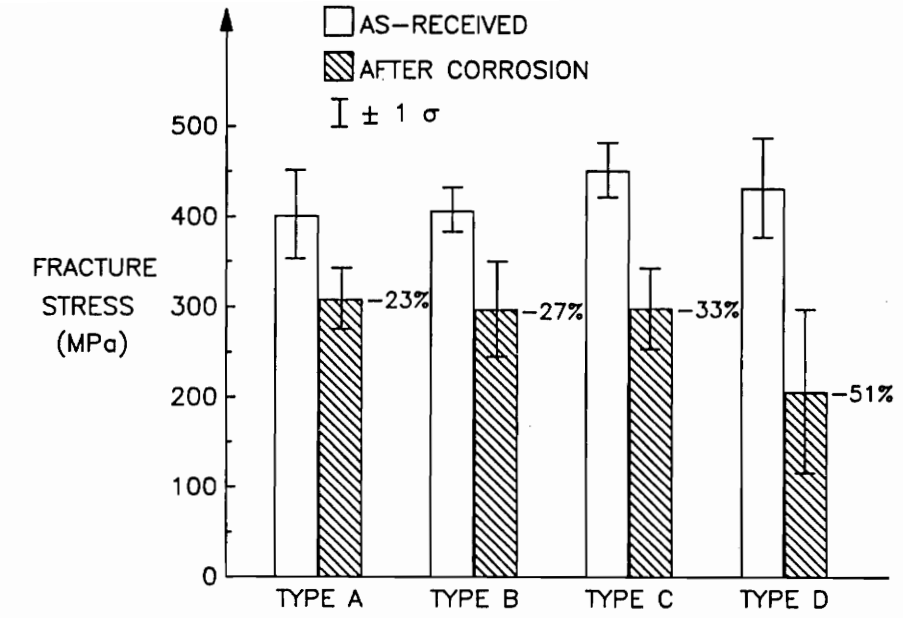

(a)

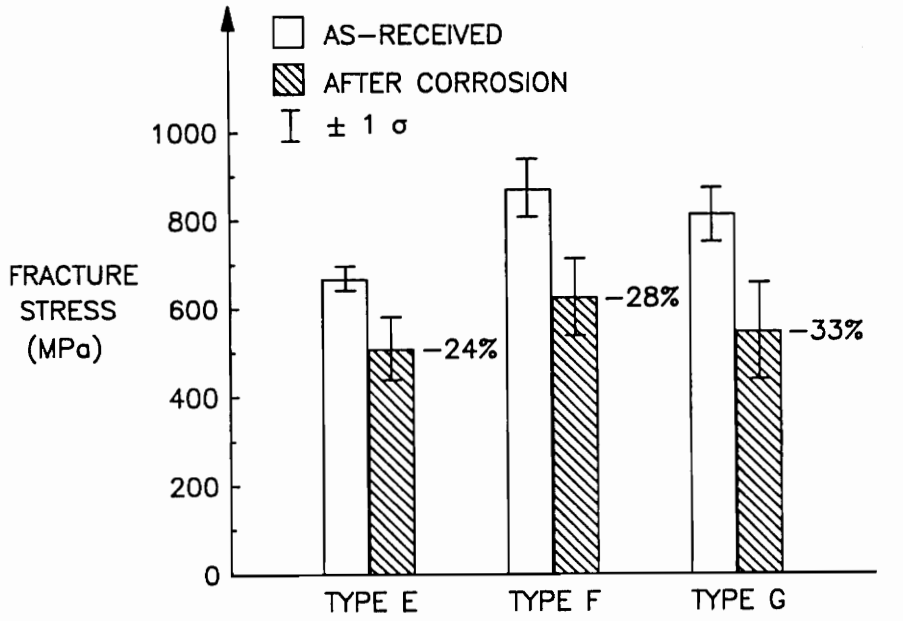

(b)

Figure 2.5: Room temperature four-point flexural strength of as-received and corroded (a) silicon carbide and (b) silicon nitride (40 h, 2 ppm Na, 1000°C, 400 kPa total system pressure) (Ref. 12)

CHAPTER 3. EXPERIMENTAL PROCEDURE

3.1 Sample Preparation

Samples of modified ß-eucryptite of composition $Li_{0.41}Mg_{0.035}AlP_{0.52}Si_{0.48}O_4$ were prepared by typical glass-ceramic techniques.

3.1.1 Single Phase Preparation

To prepare a single phase of modified ß-eucryptite, the reactant powders were mixed together and then heated to appropriate temperatures to drive off the water and other volatile products and produce the desired phase. The batch consisted of $Al(OH_3)\cdot nH_2O$, silicic acid, $MgSO_4$, Li_2CO_3, and $NH_4H_2PO_4$ (Table 3.1). A weight loss analysis was performed on $Al(OH_3)\cdot nH_2O$ and silicic acid in order to obtain the correct stoichiometry of Al_2O_3 and SiO_2. The reactant powders were mixed in acetone with a glass mortar and

Table 3.1: Reactant materials used in processing and composition of a batch receipe for 1 mole of modified ß-eucryptite.

Name	Weight Loss Factor	Weight for 1 mole (in g)	Purity
Silicic Acid	1.127	32.5032	99.9 %
Aluminium Hydroxyde	1.558	65.7462	99.8 %
Lithium Carbonate		15.1477	99.4 %
Magnesium Sulphate		4.2126	99.5 %
Amonium Phosphate		59.8135	99.9 %

pestle. After the mixture was dried, the sample was reacted by heating 2 hours at 200°C, 3 hours at 400°C, 3 hours at 800°C, 25 hours at 1070°C, and finally at 1070°C for 25 hours. After each heat treatment, the samples were thoroughly mixed in acetone with a glass mortar and pestle or in alcohol in an alumina jar mill.

At the end of this process, a crystalline single phase of modified ß-eucryptite was obtained. XRD was used to identify the phases. The resulting material was modified ß-eucryptite and often a small amount of secondary phase, $AlPO_4$ or silica, was observed. Once the solid state reaction was complete, 6 weight percent of nucleating agent, either TiO_2 or ZrO_2, was added. The samples were then melted in a vertical tube furnace at 1620°C for 3 hours. The glass was drawn into rods with a diameter of 5 mm or was quenched in water. Then different types of recrystallization methods were used to obtain a dense glass-ceramic.

3.1.2 Recrystallization Methods

Conventional recrystallization was achieved by heat-treating the rods of glass at 1000°C for 1 hour in alumina boats. DTA showed a strong exothermic peak around 800°C and thermal expansion analysis of the glass showed a peak and a large change in thermal expansion coefficient between 750°C and 850°C. These analyses indicated that the recrystallization occurs between 750°C and 850°C. A recrystallization temperature of 1000°C was chosen to increase the recrystallization rate and to limit the amount of remaining glassy phase. Different heating and cooling rates were examined to minimize the formation of microcracks but it was not possible to avoid their formation, even with a

heating rate as low as 30°C/min. The samples obtained by this method will be referred to as *"conventional"*. Grain sizes between 10 and 15 μm were obtained.

Another type of recrystallization was also used. The glass was broken and ground in alcohol in an alumina jar mill until an average powder size of 5 μm was achieved. Modified ß-eucryptite was then recrystallized by either cold-pressing or slip-casting prior to heat treatment.

In the case of cold-pressing, cylindrical bars were formed by mixing the glass powder with a few drops of deionized water and pressing at 82 Kpsi followed by heat treatment (Figure 3.1). Nucleation occurred at 730°C and the glass recrystallized at 1100°C. These samples will be referred to as *"cold-pressed"*.

The slip-cast powder was mixed with acetone, and placed in a die of glass with a paper filter at the bottom (Figure 3.2). When most of the acetone was removed but before it was completely dry, the samples were heat treated (Figure 3.1).

When 6 weight percent of TiO_2 was used as a nucleating agent, some TiO_2 fibers (rutile) formed in a matrix of modified ß-eucryptite. These fibers had an average diameter of 1 - 5 μm and a length between 10 μm and 20 μm depending on the recrystallization process. These samples will be referred to as *"slip-cast (TiO_2)"*.

Lastly, when 6 weight percent of ZrO_2 was used as a nucleating agent, no formation of fibers was observed. These samples will be referred to as *"slip-cast (ZrO_2)"* .

Table 3.2 summarizes the different samples evaluated for corrosion resistance.

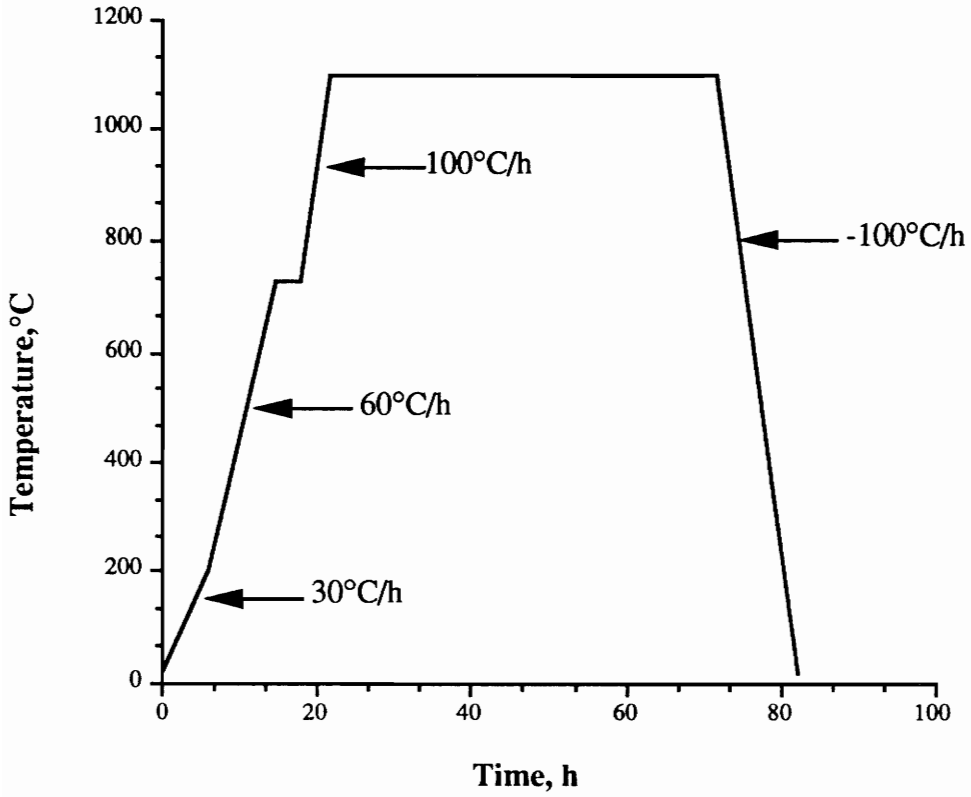

Figure 3.1: Heat Treatment Schedule (Ref. 25)

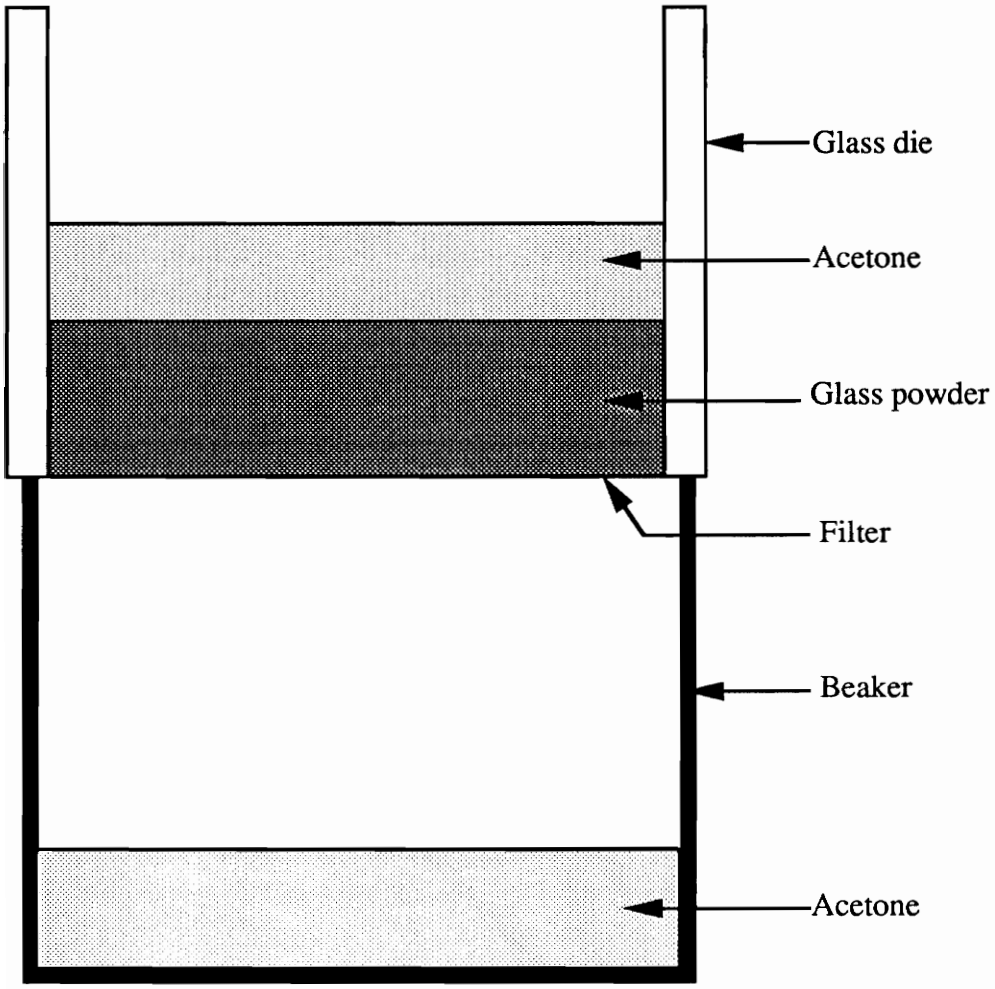

Figure 3.2: Slip-casting Process (Ref. 25)

Table 3.2: Sample descriptions

Sample Name	Manufacturing Technique	Nucleation Agent
Conventional	Recrystallization at 1000°C	ZrO_2
Cold-pressed	Grinding of the glass, cold-pressing, and then heat-treatment	ZrO_2
Slip-cast (TiO_2)	Grinding of the glass, slip casting, and then heat-treatment	TiO_2
Slip-cast (ZrO_2)	Grinding of the glass, slip-casting, and then heat-treatment	ZrO_2

3.1.3 Commercial LAS

Corrosion tests were also performed on commercial LAS. The commercial LAS was obtained by Garret Auxiliary Power Division, Allied Signal Corp., Phoenix, AZ. It consisted mainly of a ß-spodumene (Li_2O-Al_2O_3-$4SiO_2$) glass ceramic.

3.2 Corrosion Tests

3.2.1 HCl Corrosion

The samples were polished prior to corrosion with 1μm alumina. They were weighed before and after corrosion. HCl corrosion tests were performed by immersing the samples in aqueous hydrochloric acid at various concentrations and temperatures. Hydrochloric acid of pH-1.1 (normality 12.1) was used. Tests at pH-1.1, pH1, pH2, and pH4 and from room temperature to 100°C were conducted up to 1000 hours.

3.2.2 Na_2SO_4 corrosion

Corrosion tests were also performed with molten sodium sulfate. Sodium sulfate was dissolved in deionized water to saturation. The solution was then heated at 100°C, and the samples were immersed in the solution. Prior to immersion, the samples were polished with 1μm alumina, and weighed. The samples were weighed after drying, to determine if the Na_2SO_4 coating was between 4 and 6 mg/cm^2. The samples were then placed in an alumina boat in a furnace at 1000°C for several hours. This temperature had been chosen

because Na_2SO_4 melts at approximately 900°C and preliminary tests indicated the attack to be more severe at 1000°C. An alumina boat full of sodium sulfate was also placed in the furnace to slow the rate of evaporation of Na_2SO_4 from the surface of the sample. After corrosion, the samples were washed in boiling water for one hour prior to examination in order to remove the Na_2SO_4 and the soluble corrosion products.

3.3 Characterization

3.3.1 Linear Thermal Expansion

The influence of corrosion on the thermal expansion behavior of modified ß-eucryptite was investigated using a Netzsch Dual Push Rod Differential Dilatometer Model-II with an Al_2O_3 reference. A sapphire rod was used to correct for system errors and a software package computed a coefficient of thermal expansion. The relative expansion was measured between 30°C and 1000°C with a heating rate of 10°C/min. Measurements were also taken during cooling in order to observe the hysteresis phenomenon. Bar samples of 5 mm diameter and 25 mm length were tested after corrosion to monitor the effects of corrosion.

3.3.2 SEM and EDX Analysis

Scanning Electron Microscope analyses was performed on a Jeol JSM-35C microscope. Samples were coated with a 200 Å layer of gold, and an accelerating voltage

of 15 kV was used. Because of high porosity of the sample surface after corrosion, some charging was observed.

Energy Dispersive X-rays Analysis was used to characterize the samples and to determine the degree of corrosion. A Kevex EDX spectrometer was coupled with the Jeol SEM, and a Kevex software package was used to analyze the spectrum by deconvolution of the intensities giving the weight percent and the atomic percent. Only elements of atomic number greater than 10 can be detected by this method. Thus, lithium and oxygen could not be identified, but analyses of aluminum, silicon, phosphorus, zirconium and titanium were made. A typical spectra for modified ß-eucryptite with ZrO_2 and TiO_2 nucleating agents is shown in Figure 3.3. Although EDX is not a precise technique for determining the element concentration, the weight percents obtained for non-corroded samples, were in accordance to what was expected by calculations with a margin of error less than 5 percent. Elemental X-ray mapping was also done on some fracture surfaces using another Kevex software package.

3.3.3 Mechanical Tests

Mechanical tests were performed in order to compare some mechanical properties before and after corrosion tests. Bending tests were performed on an Instron 4204 testing machine to determine the modulus of rupture (MOR) and Young's modulus (E). Samples were obtained by slip casting and were 3mm x 4mm x 50mm. They were polished with 0.1µm alumina grains. Three point bending tests were performed using a 40 mm span, a 4500 N load cell and a constant crosshead speed of 0.51 mm/min. The following equation was used to compute the MOR in MPa (ASTM C203-85):

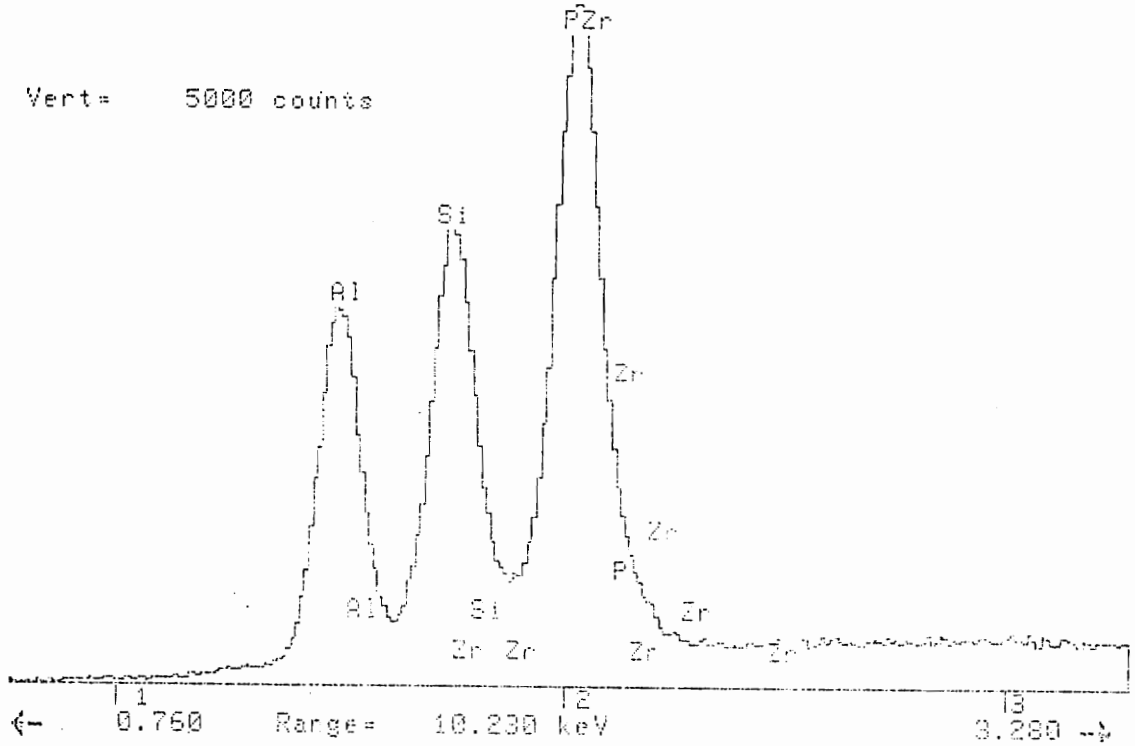

a)

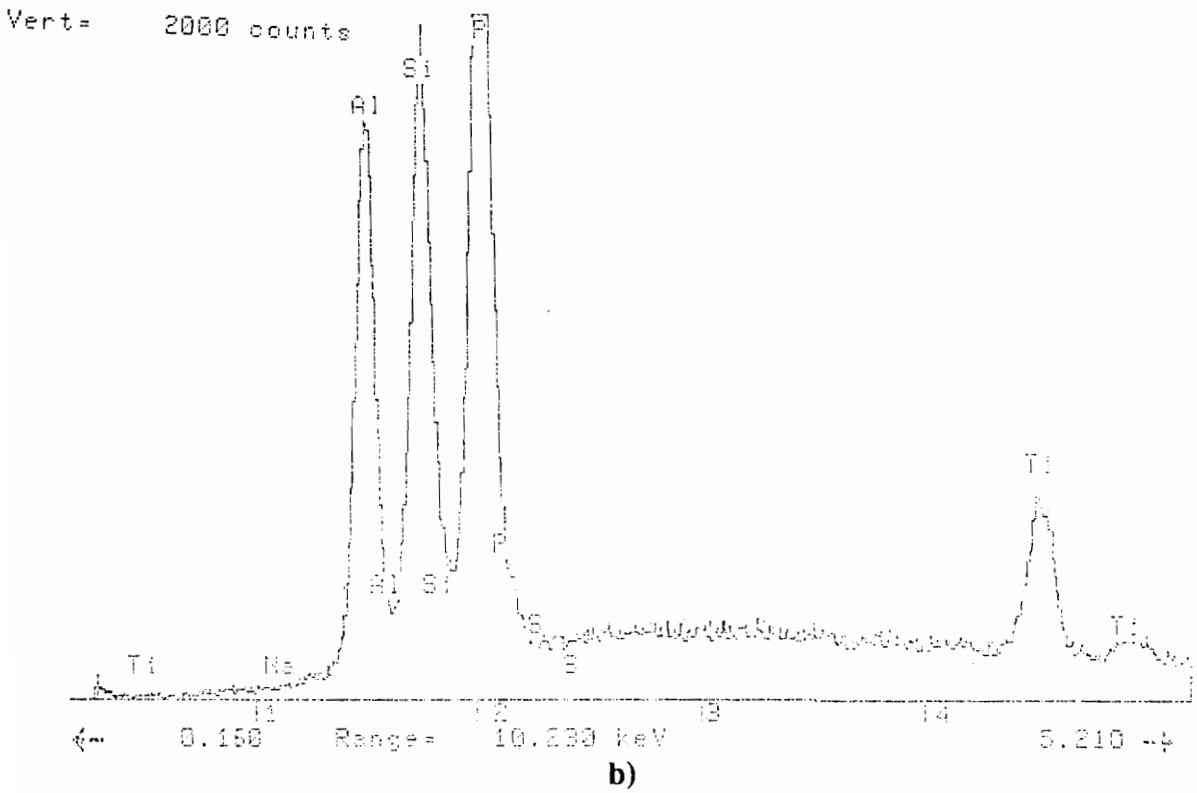

b)

Figure 3.3:EDX spectra of modified ß-eucryptite with
a) 6 wt % of ZrO_2
b) 6 wt % of TiO_2

$$MOR = \frac{3}{2}\frac{PS}{WT^2}$$

where P is the load at fracture (N), S is the span size (mm), W is the width of the specimen (mm), and T is the thickness of the specimen (mm).

The Young's modulus was calculated using the following equation in MPa:

$$E = \frac{1}{4}\left(\frac{S^3}{WT^3}\right)\frac{P}{D}$$

where D is the displacement (mm).

CHAPTER 4. RESULTS AND DISCUSSION

4.1 Characterization of the Samples

Before corrosion testing, phase identification, homogeneity, density, and thermal cycling effects were evaluated.

4.1.1 X-ray Diffraction

The X-ray pattern of the samples was determined by grinding the samples into a very fine powder, and analyzing them in a PW-1729 Phillips X-ray Diffractometer. The diffraction patterns were compared with the ones listed for pure ß-eucryptite in the Joint Committee on Powder Diffraction Standards (JCPDS) files (No. 26-839). Because the composition was modified compared to pure ß-eucryptite, the 2θ angles observed were slightly bigger than the ones listed for pure ß-eucryptite. A very small secondary phase was observed for most of the samples, corresponding to either $AlPO_4$ or silica.

4.1.2 Homogeneity

Because the surface played an important role in the corrosion process, it was important to investigate the homogeneity of the samples being tested. EDX was used to examine composition differences between the surface and the center of the conventional samples. The composition was the same from the edge of the sample to the center.

4.1.3 Density

Bulk density were measured using the standard ASTM C20-87 method. Bulk density of commercial LAS was 99.5% of theoretical. Modified ß-eucryptite had different bulk densities, depending on the manufacturing process. Conventional samples showed 99% of theoretical density, whereas cold-pressed samples were only 80-85% of theoretical density. Slip cast samples had bulk densities, between 90 and 98% of theoretical.

4.1.4 Thermal Cycling

The effect of thermal cycling during corrosion tests was examined. These tests where conducted by placing conventional samples in the form of rods (4mm x 4mm x 25mm) in the differential dilatometer and cycling them from room temperature up to 1000°C at a heating rate and cooling rate of 10°C per minute.

These tests showed a slight difference in the thermal expansion coefficient between first and second thermal cycle: from -7×10^{-7}/°C to -9×10^{-7}/°C. This is probably due to some

recrystallization which occurred during the first thermal cycle. Thereafter the thermal expansion coefficient stabilized at a value of $-9 \times 10^{-7}/°C$ (Figure 4.1).

4.2 Corrosion by HCl

4.2.1 Weight Loss

Corrosion tests in HCl pH1 at room temperature were used to compare the weight loss factor of samples prepared by different techniques. Conventional, cold-pressed, slip-cast (TiO_2) and slip-cast (ZrO_2) were tested. Corrosion tests were also performed on commercial LAS.

The cold-pressed sample had a very poor resistance to corrosion as indicated in Figure 4.2.a. This is attributed to the porosity (density of 80% of theoretical) of this material which increased the effective surface in contact with HCl, and thus decreased the corrosion resistance.

The slip cast samples appeared to be less corrosion resistant than the conventional samples (Figure 4.2.b); they have higher weight loss per unit area. But as it is shown in Figure 4.2.a, the conventional samples disintegrated after 150 hours, whereas the slip cast resisted corrosion for longer time and the weight loss factor stabilized after 400 to 500 hours. This difference in the corrosion behavior can be explained by the presence of microcracks in the conventional samples. These microcracks formed due to the large difference in thermal expansion between the parent glass and the crystalline phase during the recrystallization. These microcracks enabled the HCl to quickly penetrate the samples and

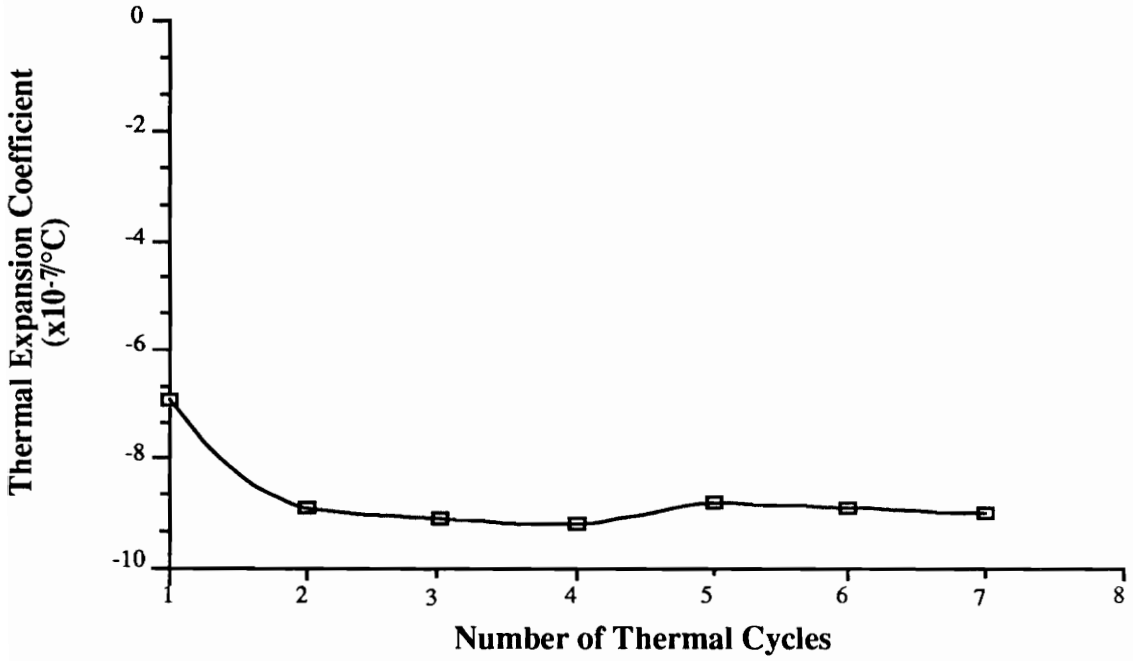

Figure 4.1: Influence of cycling on thermal expansion

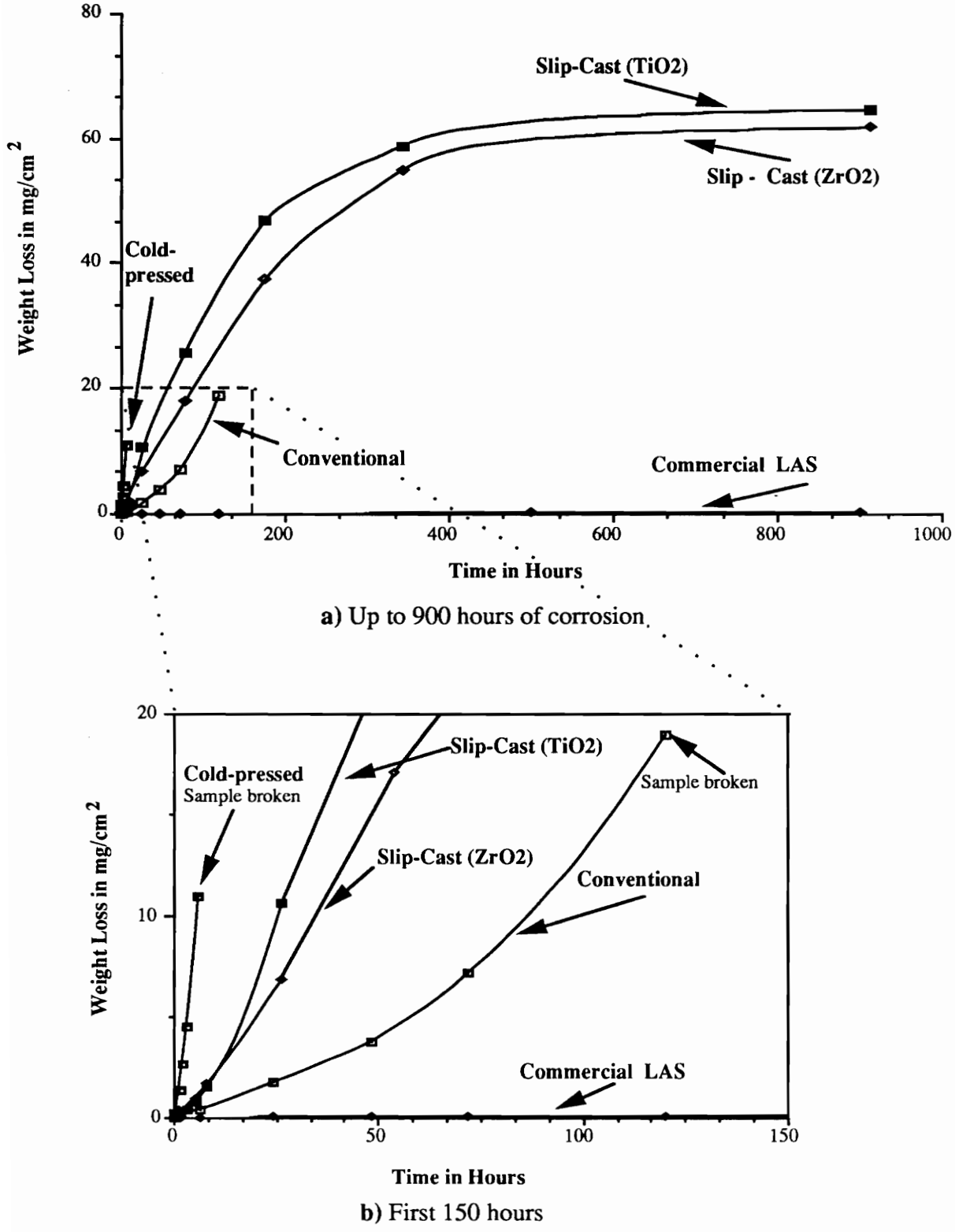

Figure 4.2: Weight Loss for Glass-Ceramic at 20°C in HCl pH 1

corrode them. This led to disintegration of the samples after short corrosion times. In contrast, the slip cast samples did not have any microcracks, and thus the rate of corrosion decreased as the corrosive layer formed. In comparison, commercial LAS did not corrode when exposed of HCl.

4.2.2 SEM and EDX Analysis

Conventional, cold-pressed, and slip-cast samples were examined. The structural difference between slip-cast (ZrO_2) samples and slip-cast (TiO_2) samples will be discussed in section 4.3.2.

Examination of corroded surfaces using SEM showed that the corrosion begins at the grain boundaries, and then, engulfs the whole grains with increasing corrosion times for all the different types of samples (Figure 4.3). The advancement of the corrosion is clearly seen in Figure 4.4, where on one side of the micrograph, the conventional sample was completely corroded, and on the other side the corrosion began along the grain boundaries and the microcracks. This process transformed the dense and non-porous ceramic into a very porous ceramic with a collapsed structure. The corroded layer can be clearly observed as illustrated in Figure 4.5: on the external part of the samples, the corroded layer has a thickness of 0.15 mm for a conventional sample etched 1 hour in HCl pH-1.1 at room temperature (Figure 4.5.a) and a thickness of 0.40 mm for a conventional sample etched 1 hour in HCl pH-1.1 at 100°C (Figure 4.5.b). An intermediate layer is observed which consists mainly of an etched glassy phase while the center of the rod is uncorroded.

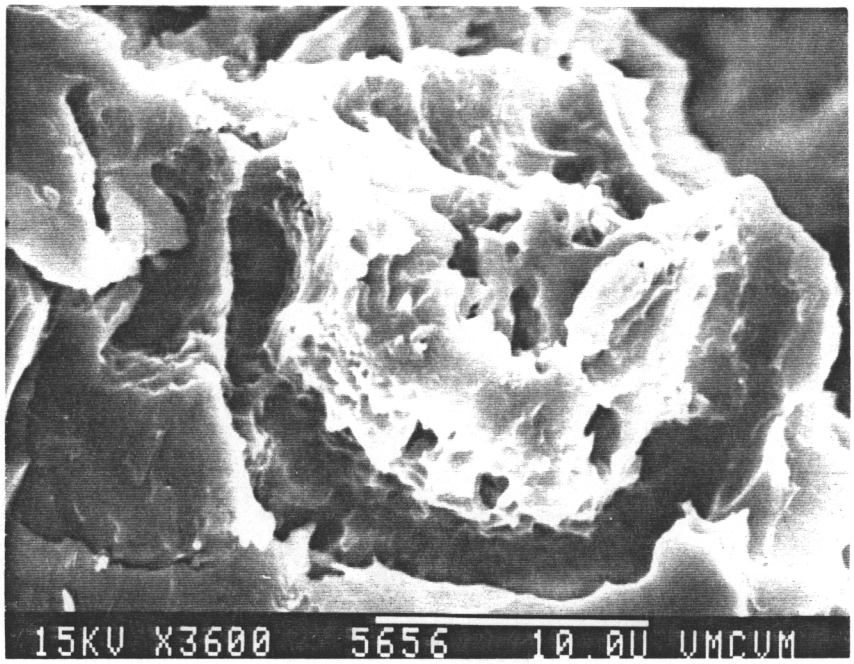

Figure 4.3: Modified ß-eucryptite (conventional) etched in HCl pH-1.1 at 100°C for 20 minutes (magnification x3600)

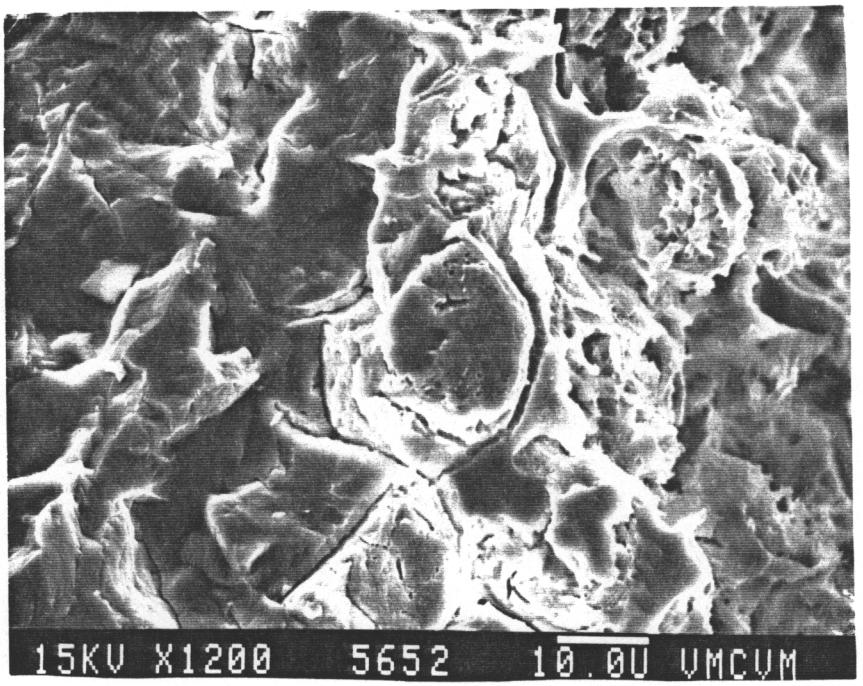

a)

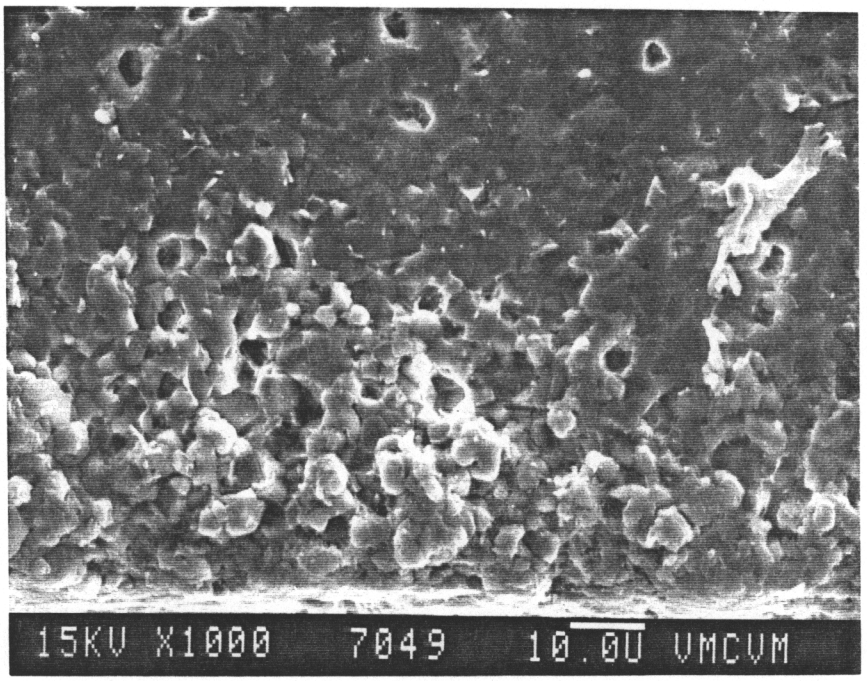

b)

Figure 4.4: Modified ß-eucryptite etched in HCl pH-1.1 at 20°C
a) conventional sample, 20 minutes, surface on the right
b) slip cast (ZrO_2) sample, 2 hours, surface on the bottom

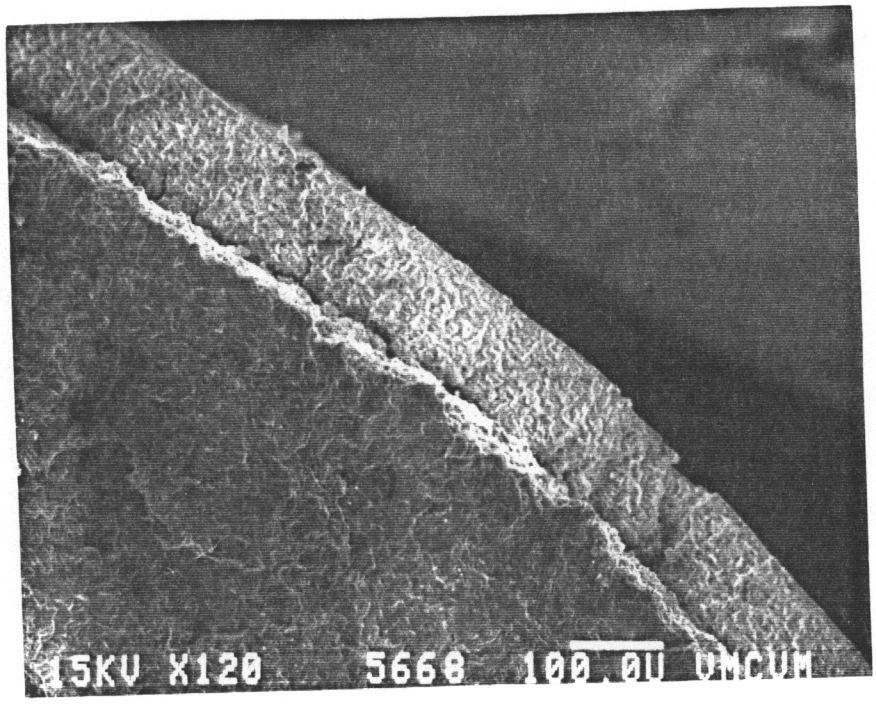

a)

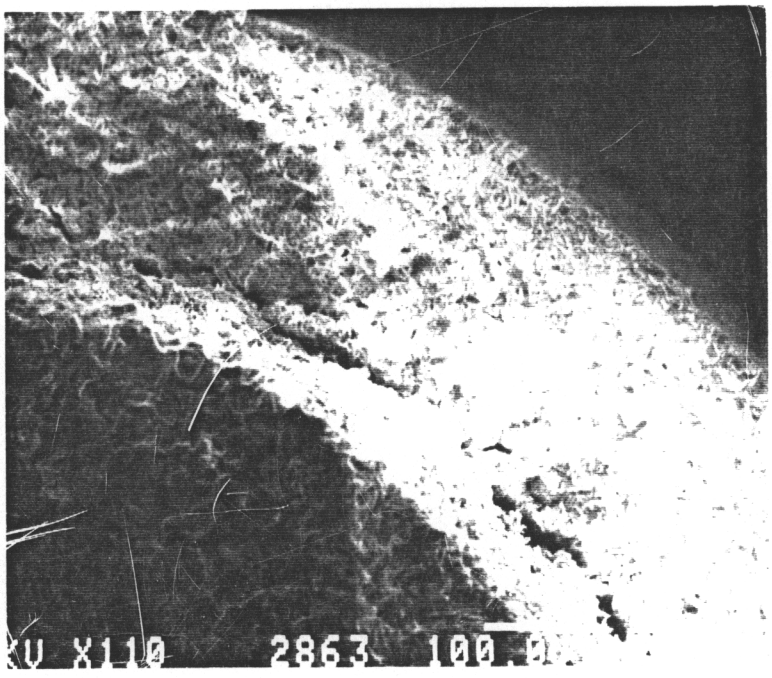

b)

Figure 4.5: Modified ß-eucryptite (conventional) etched for 1 hour in HCl pH-1.1
a) at 20°C
b) at 100°C

The analysis using an XRD of the external part indicated that it is a glassy phase (no peaks were detected). This external layer was also analyzed using EDX to quantify the variations in the composition. Figure 4.6.a shows an EDX spectra of a sample surface before exposure to HCl with predominantly aluminum, silicon, phosphorus and zirconium peaks. The EDX spectra of a sample surface after corrosion for 10 minutes in HCl pH-1.1 at 100°C shows small aluminum, phosphorus and zirconium peaks. Only silicon remains on the surface (Figure 4.6.b).

An EDX analysis was done on a fractured conventional sample in a window of 80 μm x 200 μm, every 80 μm, from the corroded surface to the non-corroded center of the specimens. This sample had been exposed for 10 minutes to HCl pH-1.1 at 100°C. The atomic percentage of each element was calculated and plotted against the distance from the surface (Figure 4.7). It indicates that aluminum and phosphorus were leached from the surface.

EDX analysis of the surface of conventional, cold-pressed and slip-cast samples exposed to HCl pH-1.1 at 100°C for various times again showed the removal of aluminium and phosphorus. Figure 4.8 represents the variation of the atomic percentage of the analyzed elements versus the corrosion time. It can be seen that after 10 minutes of corrosion, most of the aluminum and phosphorus were etched away and that after 30 minutes, the composition stabilized on the surface of the samples. With increasing corrosion time however, the thickness of the corroded layer increased. X-ray mapping was also performed confirming these results (Figure 4.9). Thus $AlPO_4$ appears to be the first component to be leached by the HCl environment.

A comparison is done in Figure 4.10 between the composition of the corroded part and the non-corroded part of cold-pressed modified ß-eucryptite and of commercial LAS.

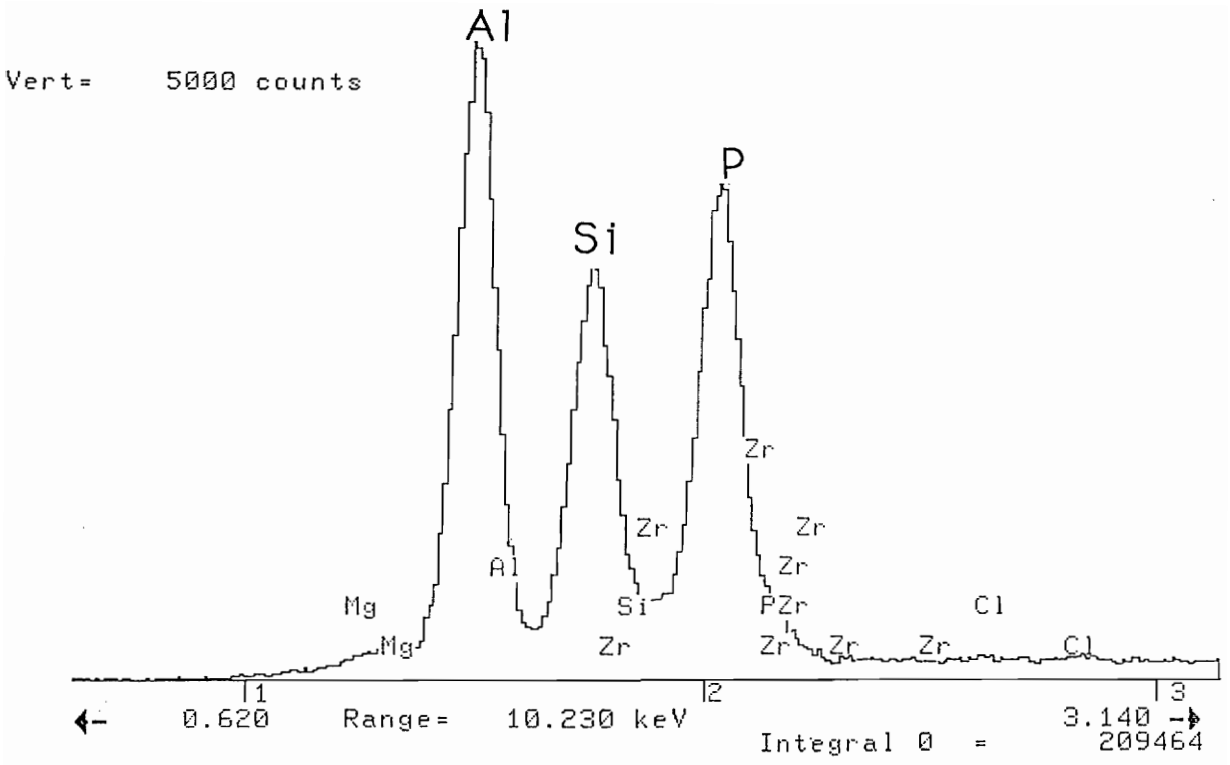

a)

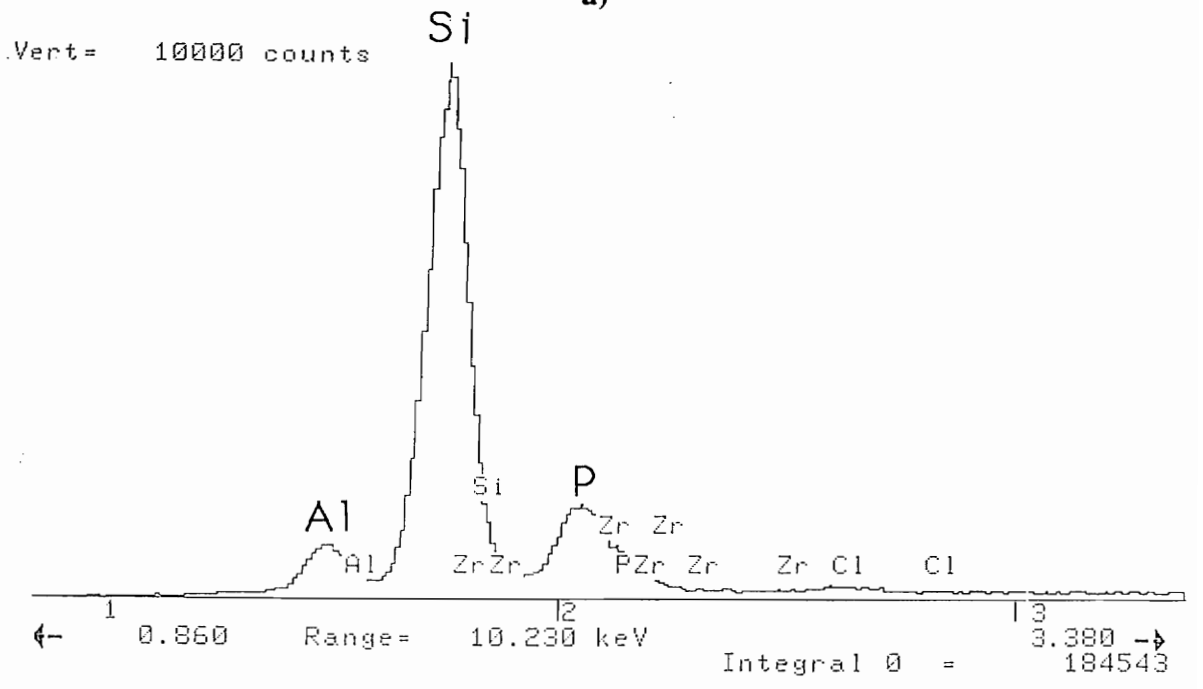

b)

Figure 4.6: EDX spectra of the surface of modified ß-eucryptite after 10 minutes in HCl pH-1.1 at 100°C:
a) at the center of the rod
b) near the surface if the rod (first 80 mm)

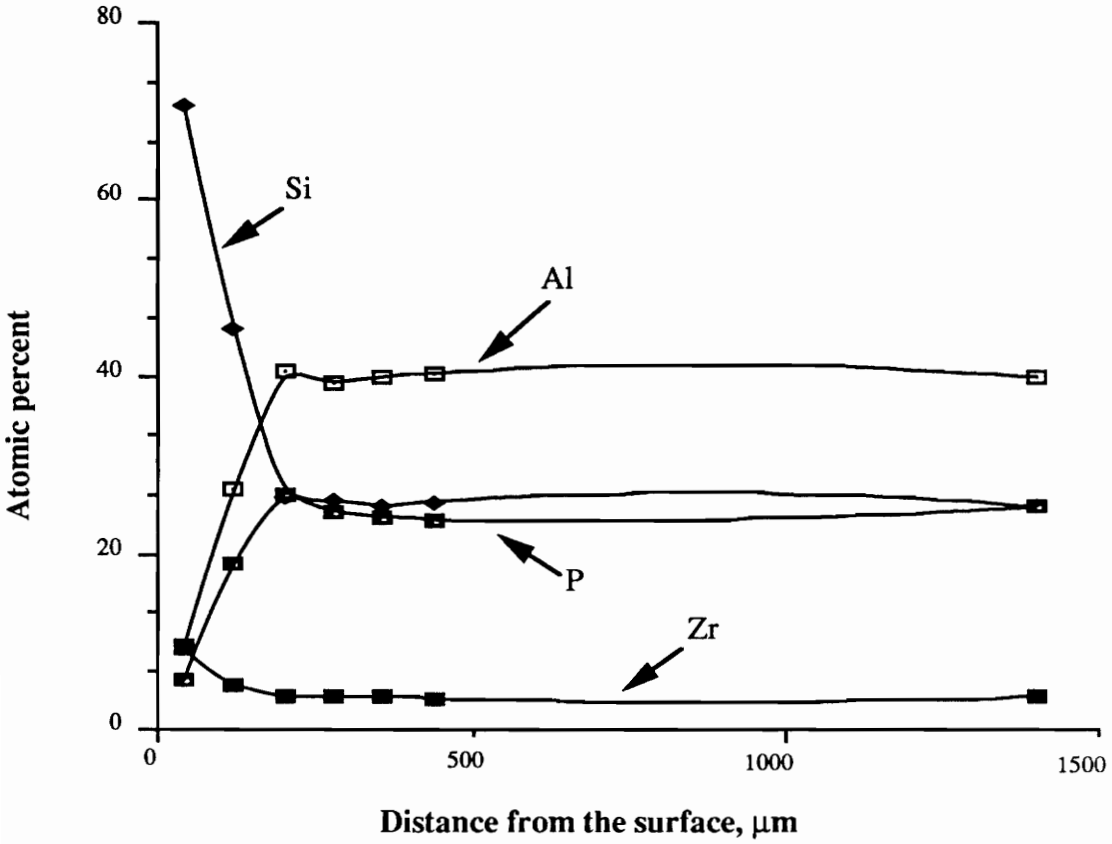

Figure 4.7: Compositional variations of modified ß-eucryptite corroded in HCl pH-1.1 at 100°C for 10 minutes (Results obtained by EDX analysis)

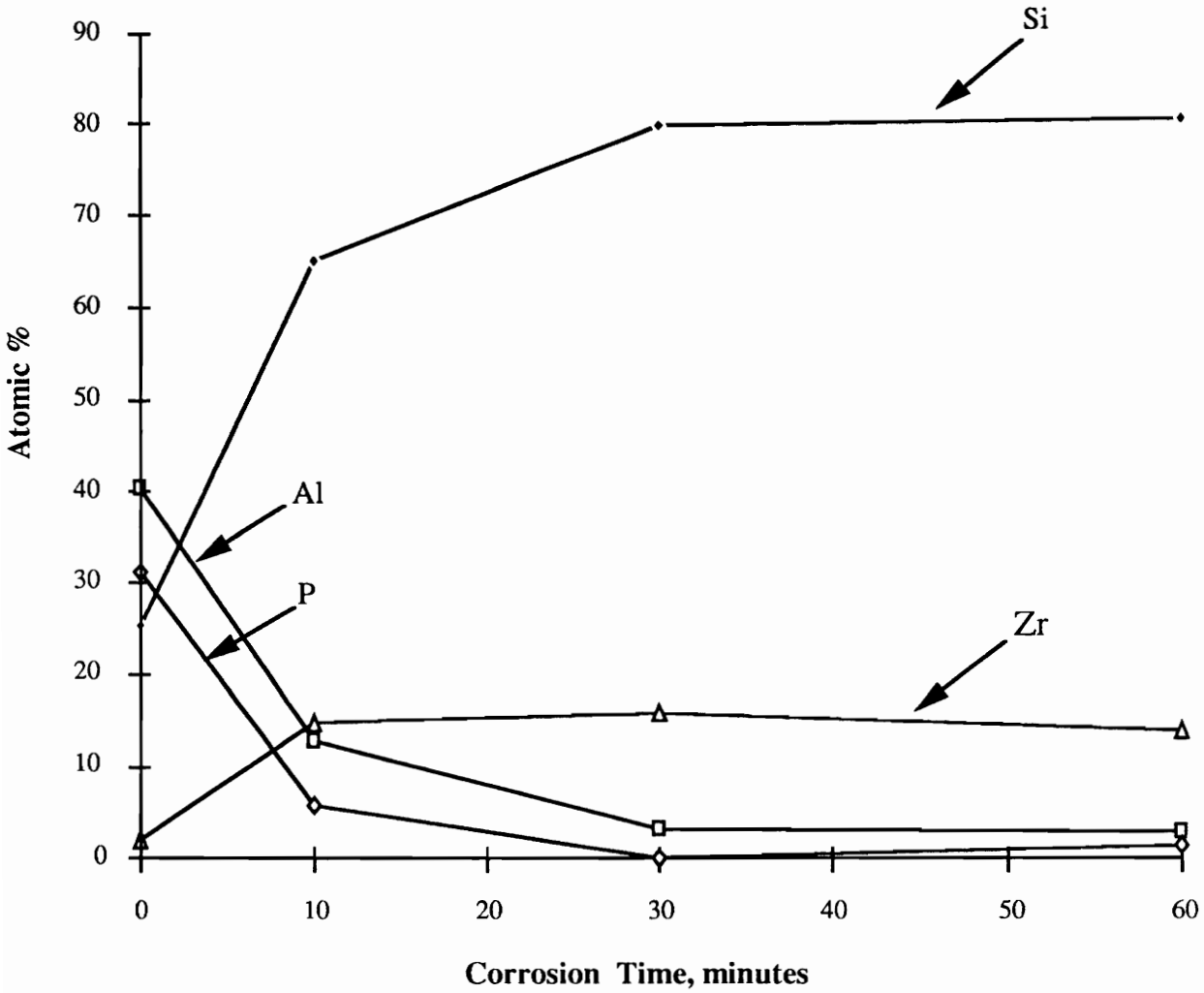

Figure 4.8: Compositional variation of modified ß-eucryptite corroded in HCl pH-1.1 at 100°C (Results obtained by EDX analysis)

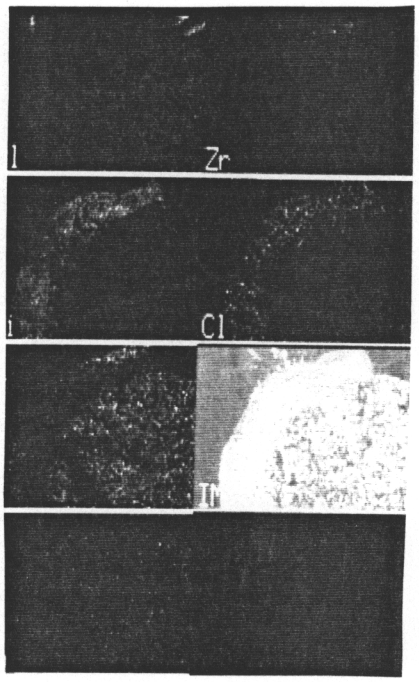

Figure 4.9: X-ray mapping of a fracture surface of modified ß-eucryptite (conventional) after 1 hour in HCl pH-1.1 at 100°C
First columm: Al, Si, P, Ti
Second columm: Zr, Cl, Image

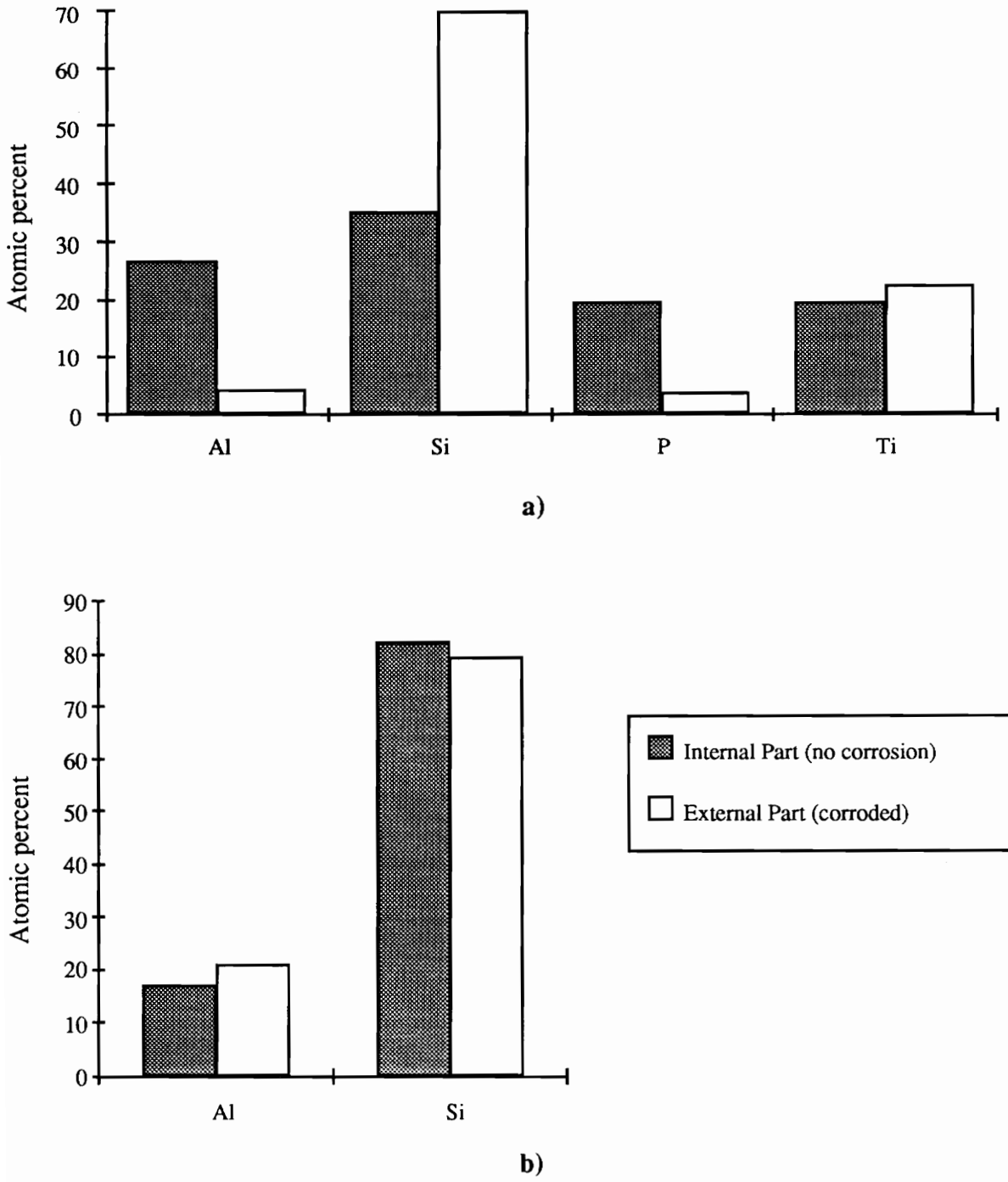

Figure 4.10: Composition obtained by EDX for :
a) Cold-pressed modified ß-eucryptite in HCl pH-1.1 at 100°C for 10 minutes
b) Commercial LAS in HCl pH-1.1 at 100°C for 5 hours

In this case TiO_2 was used as a nucleating agent for the modified ß-eucryptite. The titanium content increased with the silicon atomic percent after corrosion, while aluminum and phosphorus atomic percentages drastically decreased. In the case of commercial LAS no removal of aluminum or silicon was observed (the slight variations observed can be attributed to the margin of error of EDX analysis).

4.2.3 Linear Thermal Expansion

Coefficient of thermal expansion was measured for conventional modified ß-eucryptite. It became more negative with increasing corrosion times (Figure 4.11). With corrosion in HCl pH-1.1 at room temperature, the thermal expansion coefficient varied from $-7x10^{-7}/°C$ before exposure to $-33.3x10^{-7}/°C$ after 20 minutes in HCl.

Exposure to HCl at a lower concentration (pH1) did not significantly affect the thermal expansion coefficient as shown in Figure 4.12. When exposed to HCl solutions of pH equal to or greater than pH4, no corrosion was detected. Same observations were done with cold-pressed and slip-cast samples.

$AlPO_4$ was added to reduce the anisotropy and increase the thermal expansion coefficient of pure ß-eucryptite from a value at approximately $-70x10^{-7}/°C$ to a near zero value ($-7x10^{-7}/°C$). Therefore, the removal of $AlPO_4$ from the samples with HCl corrosion decreases the overall thermal expansion coefficient.

4.2.4 Mechanical Properties

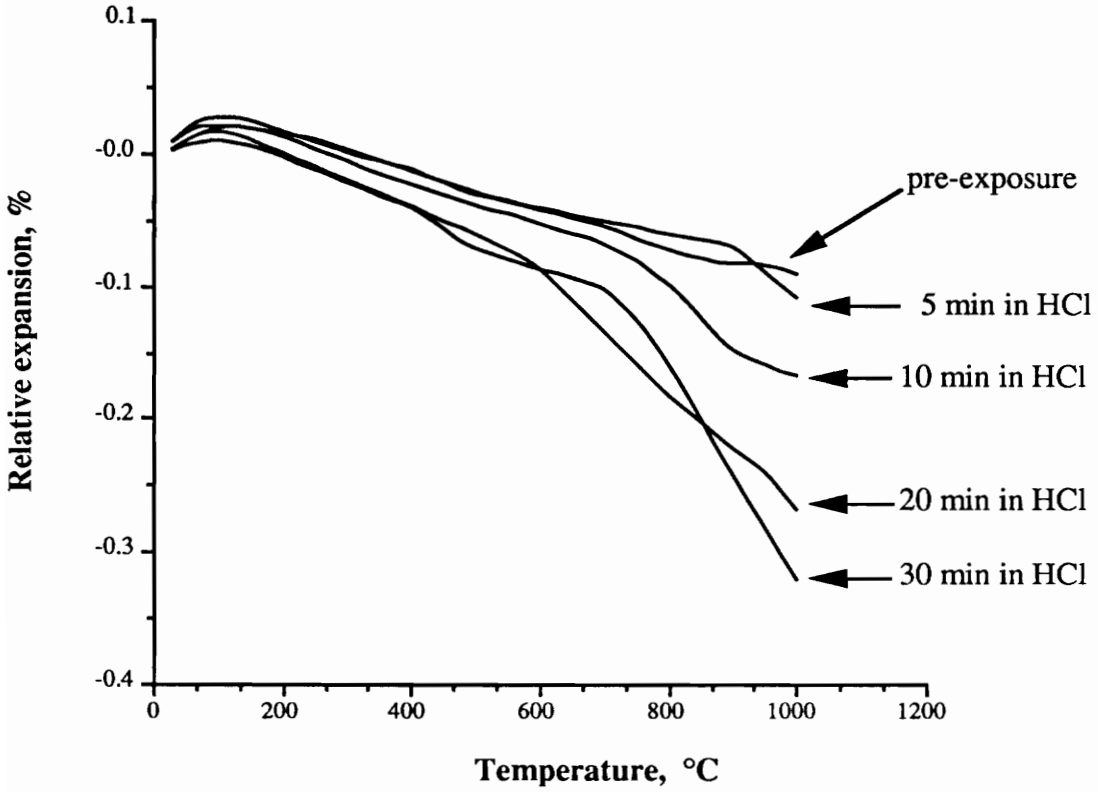

Pre-exposure:	$\alpha = -7.4 \times 10^{-7}/°C$
After 5 minutes in HCl:	$\alpha = -10.4 \times 10^{-7}/°C$
After 10 minutes in HCl:	$\alpha = -18.3 \times 10^{-7}/°C$
After 15 minutes in HCl:	$\alpha = -28.1 \times 10^{-7}/°C$
After 20 minutes in HCl:	$\alpha = -33.3 \times 10^{-7}/°C$

Figure 4.11: Relative thermal expansion of modified ß-eucryptite (conventional) in HCl pH-1.1 at 20°C for different lengths of time

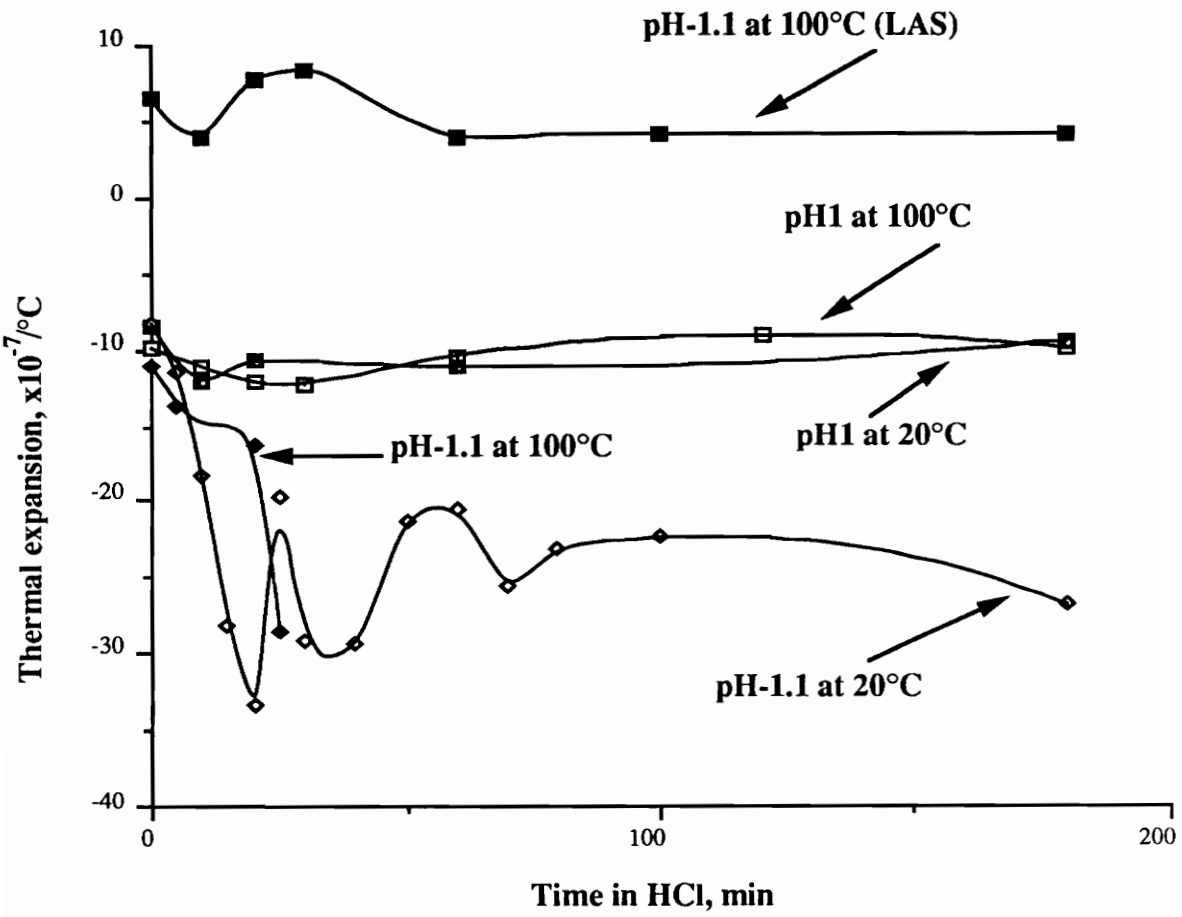

Figure 4.12: Thermal expansion coefficient of conventional modified ß-eucryptite and commercial LAS in HCl

Mechanical properties (MOR and Young's modulus) were calculated from the results of three point bending tests. Slip-cast samples were corroded for two hours in HCl pH-1.1 at room temperature. For slip-cast (ZrO_2) samples, the MOR was reduced by 20 percent, and for slip-cast (TiO_2), there was only a 16 percent reduction (Figure 4.13). This difference in the effect of corrosion on the MOR can be explained by the presence of fibers which have a strengthening effect when TiO_2 is used as a nucleating agent. Due to large standard deviation, the variation of the Young's modulus in both cases was not significant (Figure 4.14).

4.2.5 Summary

Modified ß-eucryptite obtained either by conventional method, by cold-pressing, or by slip-casting had poor corrosion resistance to HCl due to the removal of $AlPO_4$. Slip-cast samples, which exhibited high density and no microcracking were more corrosion resistant than conventional samples or cold-pressed samples. However, their corrosion resistance was still poor compared to commercial LAS. This led to a decrease in the thermal expansion coefficient and a reduction of the modulus of rupture.

4.3 Corrosion by Na_2SO_4

4.3.1 Weight Gain

Modified ß-eucryptite samples (conventional, slip-cast) and commercial LAS samples were exposed to high temperature corrosion (1000°C) by a thin salt layer of

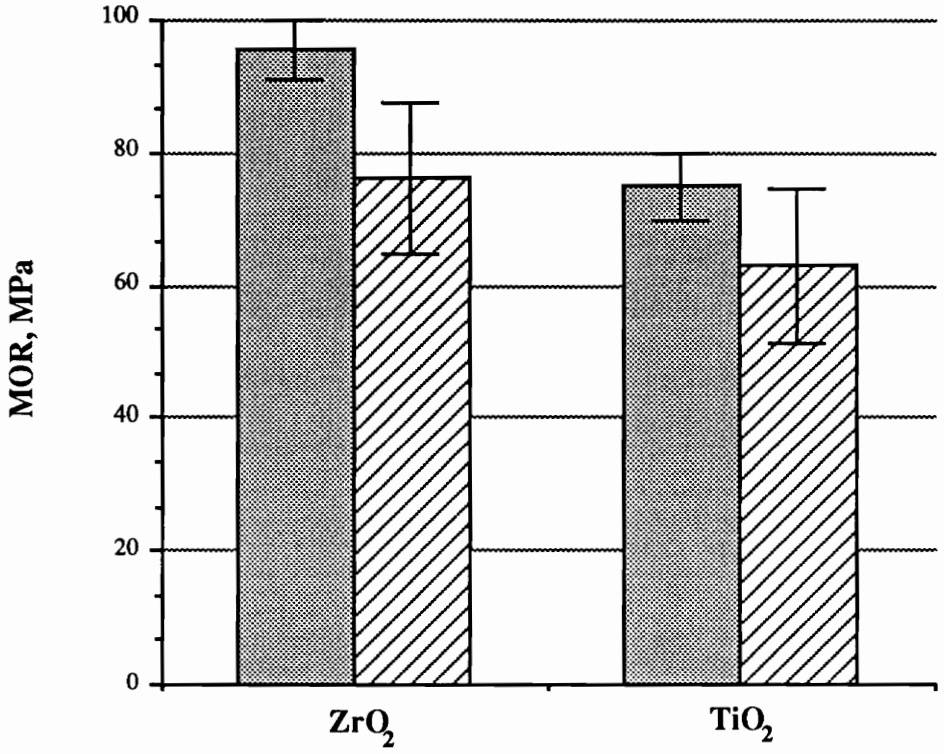

Figure 4.13: Modulus of rupture for modified ß-eucryptite (slip-cast (ZrO_2) and slip-cast (TiO_2) samples).

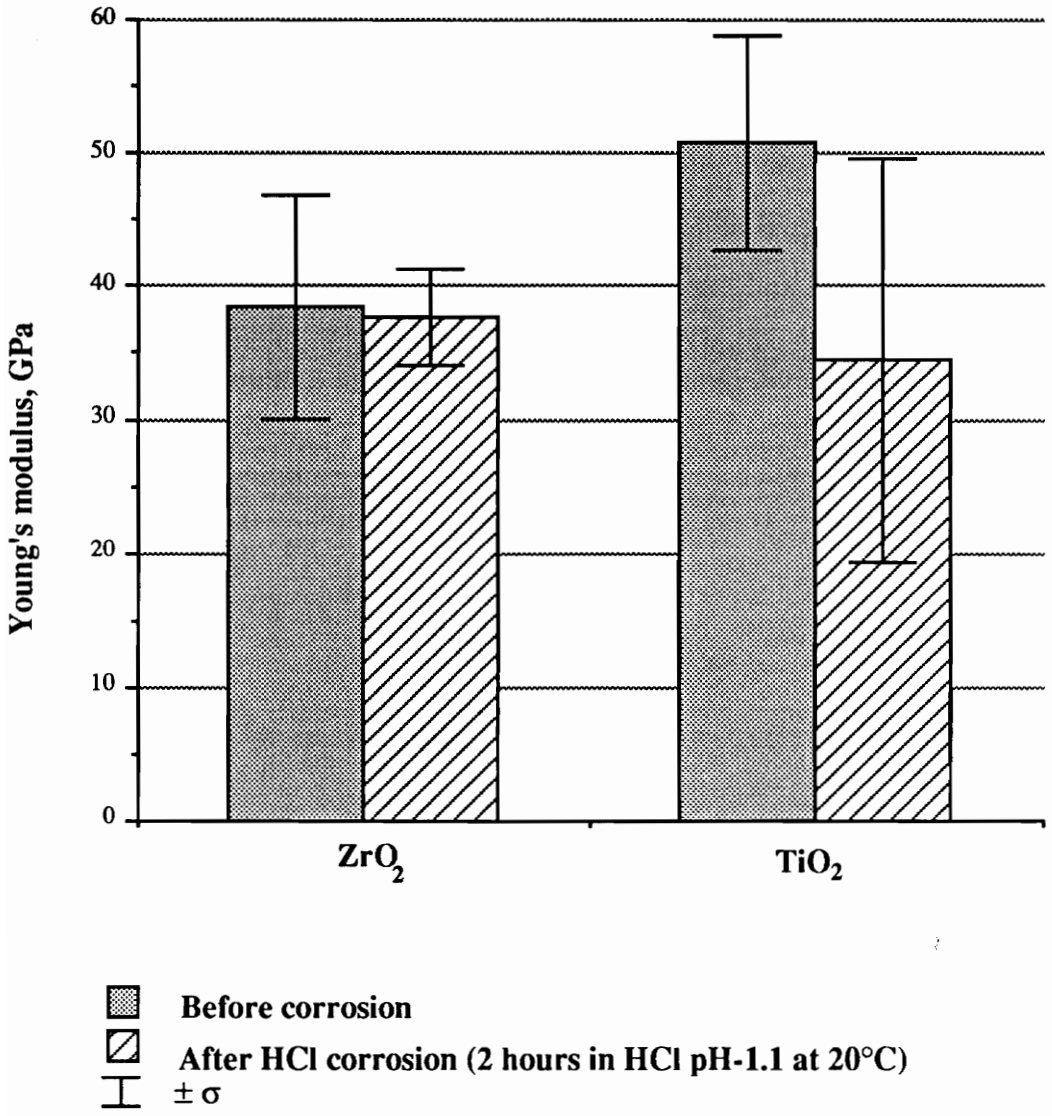

Figure 4.14: Young's Modulus for modified ß-eucryptite (slip-cast (ZrO_2) and slip-cast TiO_2) samples).

Na_2SO_4. In the case of conventional samples, a rapid destruction of the samples was observed. For the slip-cast samples as well as for the commercial LAS samples, weight gains were observed (Figure 4.15). The weight gain data was measured after the samples had been washed for one hour in boiling water in order to remove the Na_2SO_4 which could still be on the surface and to remove the water soluble corrosion products. The weight gain for the commercial LAS was less than that for modified ß-eucryptite, but was not negligible. The linear rate of corrosion for commercial LAS and the exponential rate of corrosion for modified ß-eucryptite indicated that no barrier existed for the transport of the corrosive salt through the corrosion products and the surface of the samples.

4.3.2 SEM and EDX Analysis

After high temperature corrosion, the slip-cast samples exhibited surface roughening. Some localized attacks or pitting was observed after the corrosion products were removed. When fracture surfaces of corroded samples were observed by SEM, large globules of corrosion products were found (Figure 4.16). Those globules localized between 30 and 60 µm under the surface of the sample, had sizes ranging from 0.1 mm to 0.6 mm diameter.

EDX could not be used to quantify the presence of sodium or sulfur because the peaks were too small compared to the background noise, but X-ray mapping showed the presence of sodium and sulfur under the surface (Figure 4.17). X-ray diffraction did not show the presence of a new crystalline phase on the superficial layer.

An explanation of the corrosion mechanism could be that the salt penetrates through the pores, the microcracks, and by diffusion. Modified ß-eucryptite, and commercial LAS to a lesser degree, were porous. Cold-pressed samples, which had higher porosity than slip-

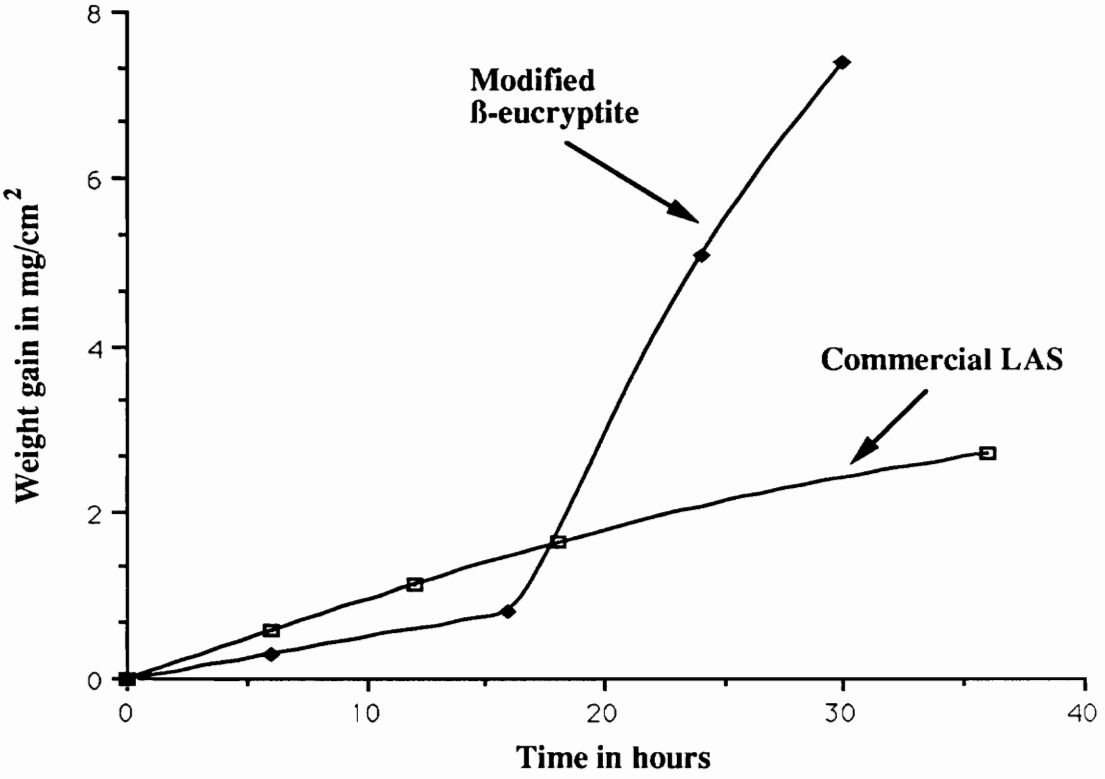

Figure 4.15: Weight gain with corrosion time for slip cast (ZrO_2) modified ß-eucryptite and commercial LAS in Na_2SO_4

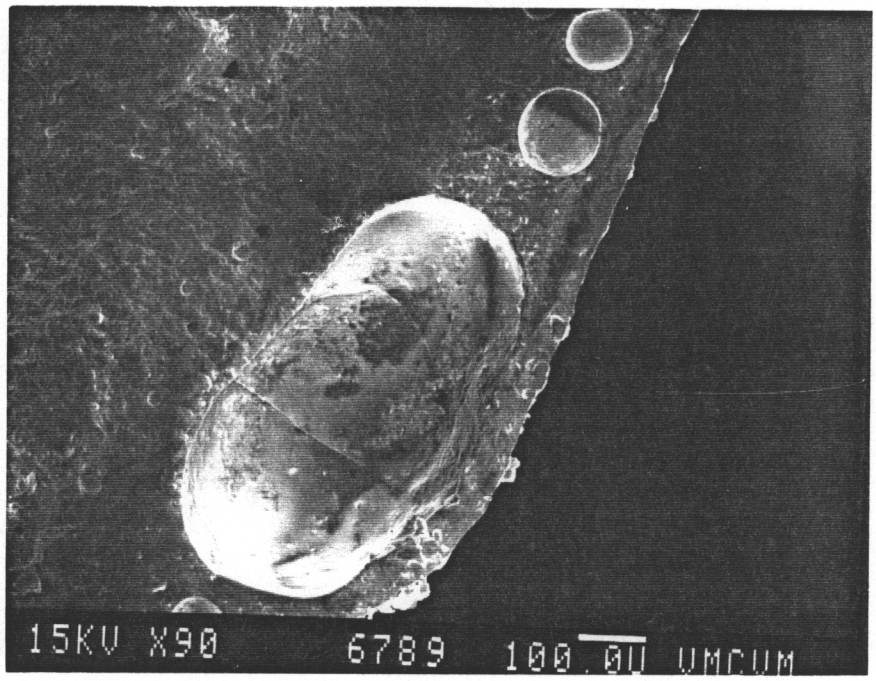

a)

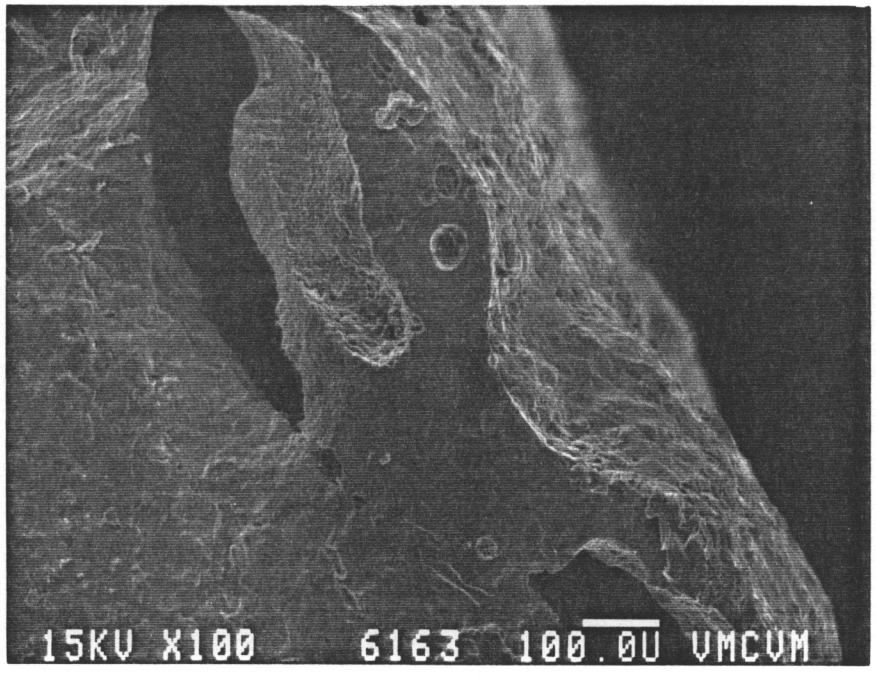

b)

Figure 4.16: Fracture surface perpendicular to the surface of samples of slip-cast (TiO_2) modified ß-eucryptite corroded by a thin layer of Na_2SO_4 at 1000°C for 54 hours:
a) as corroded
b) washed for 1 hour in boiling water

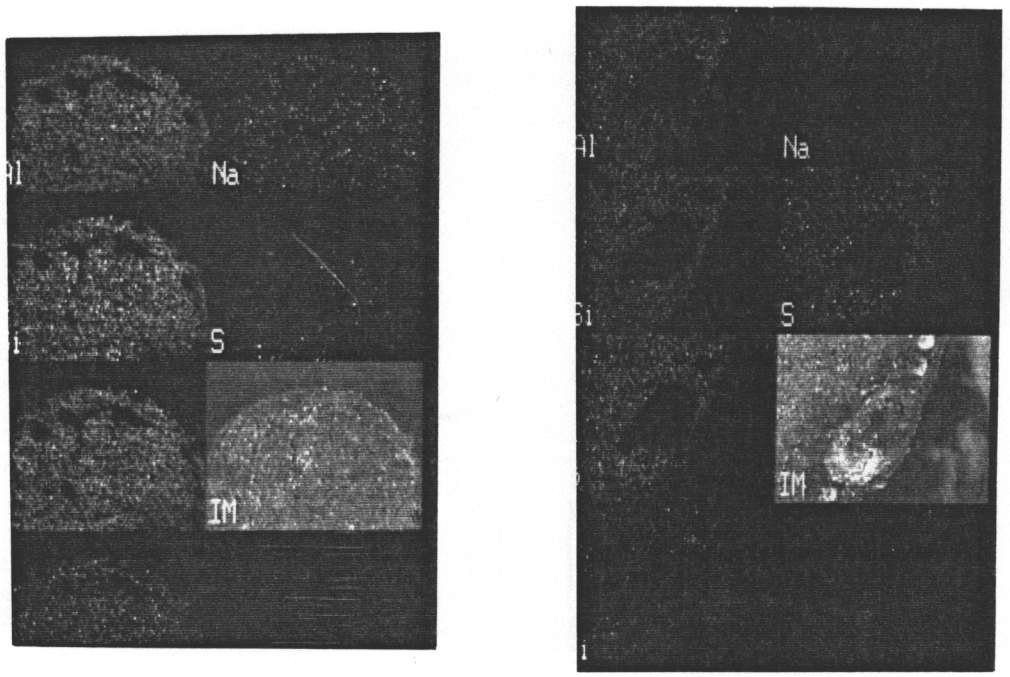

a) b)

Figure 4.17: X-ray mappings of sections perpandicular to the surface of conventional modified ß-eucryptite corroded at 1000°C by a thin film of Na_2SO_4 :
a) for 12 hours (mag x 24)
b) for 54 hours (mag x 90)
First columm: Al, Si, P, Ti
Second columm: Na, S, Image

cast samples, gained more weight. This indicated that salt penetrated through the pores. The salt seemed to react with modified ß-eucryptite to form a melt, with low melting temperatures, which concentrated in the form of bubbles. The reduction of the intensity of the peaks on X-ray diffraction of the superficial layer seemed also to indicate that modified ß-eucryptite is partially transformed to an amorphous phase during the corrosion process.

The alkali melt was washed off the surface in boiling water, and the corroded samples were examined. The morphology of the surface was very different, depending if ZrO_2 or TiO_2 was used as a nucleating agent. When ZrO_2 was used as a nucleating agent, the resulting surface was a skeleton of ZrO_2 (Figure 4.18.a), and the modified ß-eucryptite was dissolved by the melt. When TiO_2 was used as a nucleating agent, TiO_2 fibers were observed on the resulting surface (Figure 4.18.b). These fibers had an average diameter between 1 µm and 5 µm and a length between 10 µm and 20 µm. The modified ß-eucryptite matrix was also dissolved in the melt.

4.3.3 Linear Thermal Expansion

Thermal expansion tests were performed after washing the samples for one hour in boiling water. The relative expansion curves of slip-cast (ZrO_2) samples are shown before corrosion, after 6 hours, and after 30 hours of high temperature corrosion (Figure 4.19). The decrease of thermal expansion coefficient is attributed to the presence of the alkali melt.

For the corroded samples, from room temperature up to a temperature between 650°C and 700°C, the thermal expansion was near a zero value due to two opposite effects:

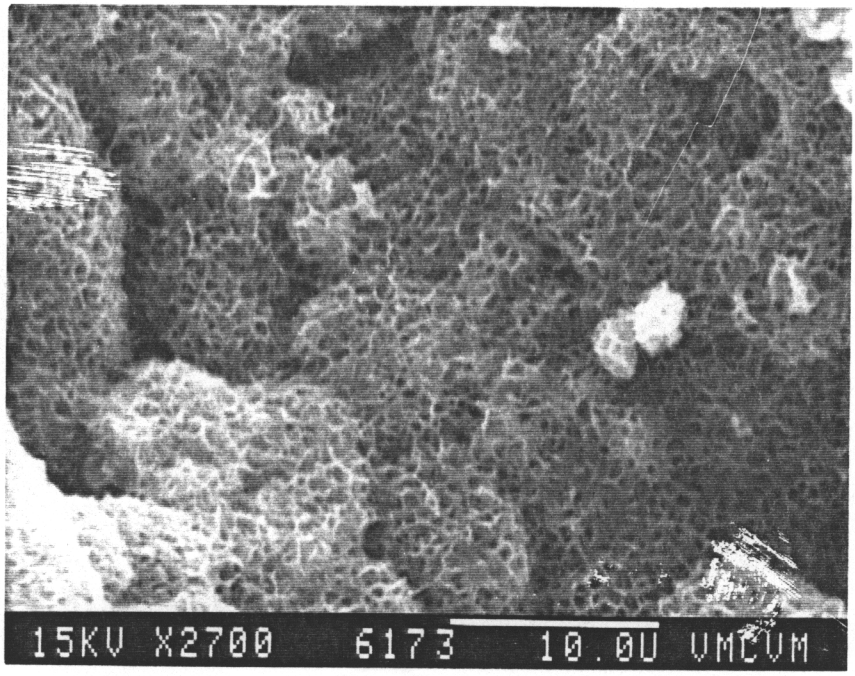

a)

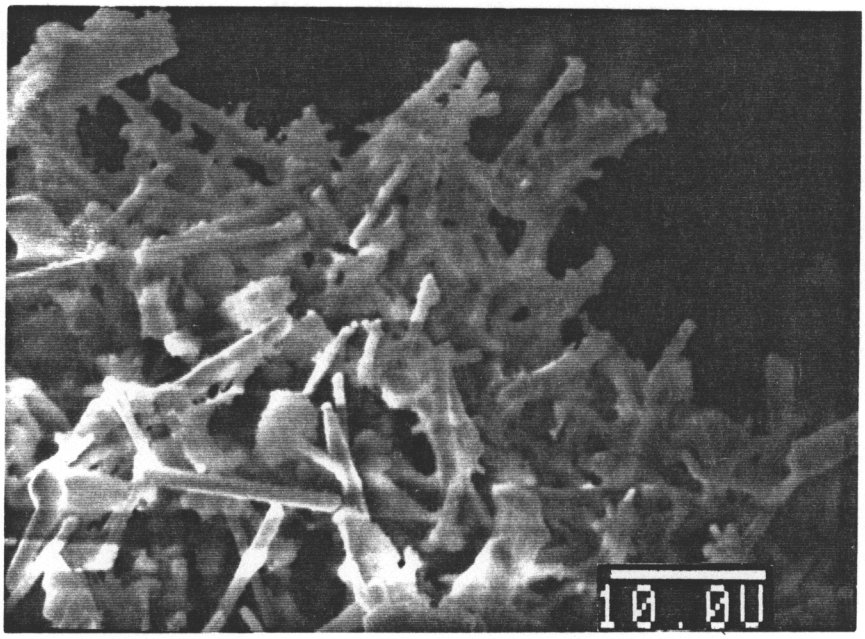

b)

Figure 4.18: SEM picture of the surface after washing in water of modified ß-eucryptite after corrosion at 1000°C for 30 hours by a thin film of Na_2SO_4
a) slip-cast (ZrO_2)
b) slip-cast (TiO_2)

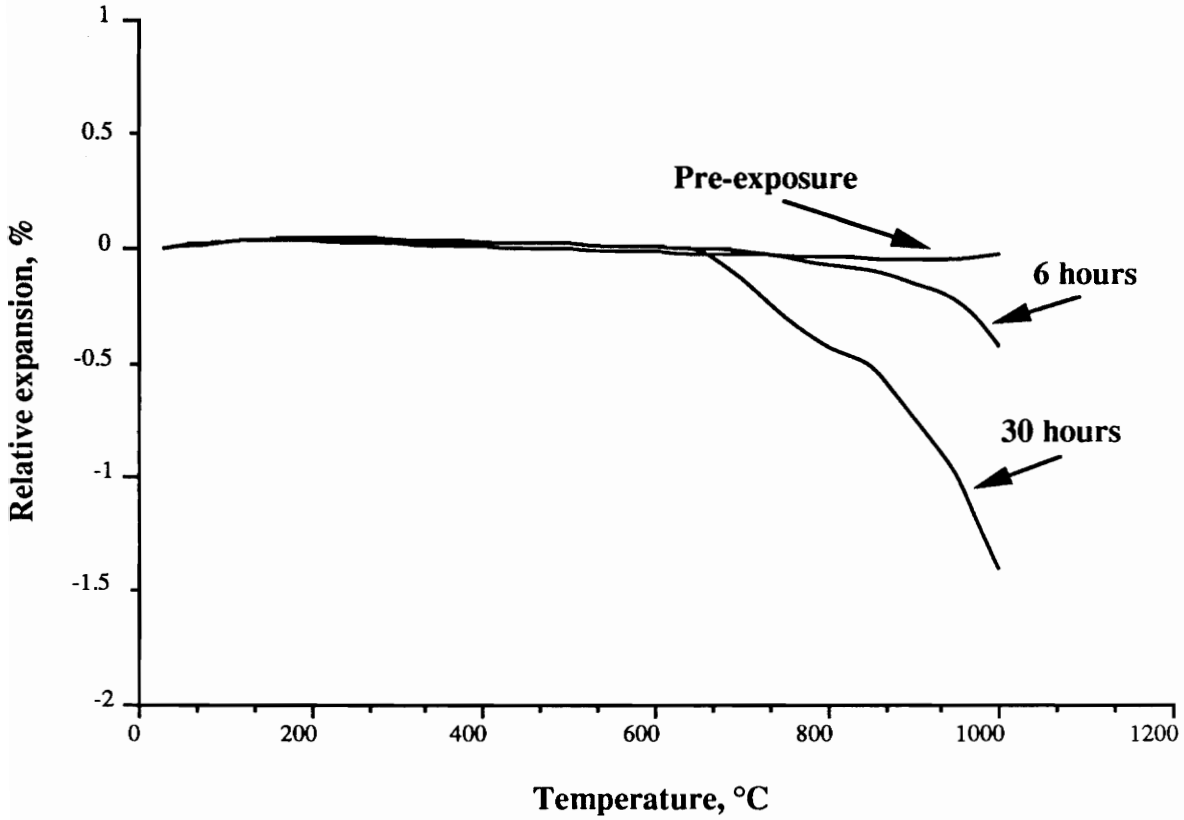

Pre-exposure:	α = -4.2 x 10^{-7}/°C
After 6 hours in molten salt:	α = -42.6 x 10^{-7}/°C
After 30 hours in molten salt:	α = -143.2 x 10^{-7}/°C

Figure 4.19: Relative expansion of slip-cast modified ß-eucryptite corroded in molten Na_2SO_4 at 1000°C

the slightly negative thermal expansion coefficient of modified ß-eucryptite ($-4.3x10^{-7}/°C$) was compensated by the positive thermal expansion of the alkali products. When the temperature was above 700°C, the alkali products melted, and because those alkali melt globules were very close to the surface, the overall thermal expansion dropped drastically to reach a value of $-143x10^{-7}/°C$ after 30 hours of high temperature corrosion. This very low thermal expansion coefficient may be explained by the viscous flow of the amorphous phase present near the surface as mentioned in the previous section.

The thermal expansion coefficient of slip-cast (ZrO_2) modified ß-eucryptite after molten salt corrosion was also compared to the one of commercial LAS (Figure 4.20). Commercial LAS had a similar behavior, with a decrease of the thermal expansion coefficient down to $-60x10^{-7}/°C$ after 36 hours of high temperature corrosion. In this case the decrease in the thermal expansion coefficient occurred after 600°C, the probable melting temperature of the formed melt. The high temperature corrosion of commercial LAS was less than that of modified ß-eucryptite and began after longer exposure time. This could be explained by the lower porosity of commercial LAS which decreased the wetting of the molten salt on the sample surface, and decreased the penetration of the corrosive salt.

4.3.4 Mechanical Tests

Three point bending tests were completed after the samples had been corroded for 24 hours at 1000°C by molten salt. This time, for slip-cast (ZrO_2) samples, the MOR decreased by 87 percent, but only by 66 percent for slip-cast (TiO_2) (Figure 4.21). This difference in the behavior in corrosive environments can here again be attributed to the presence of fibers in the case of slip-cast (TiO_2). The decrease in the Young's modulus is in

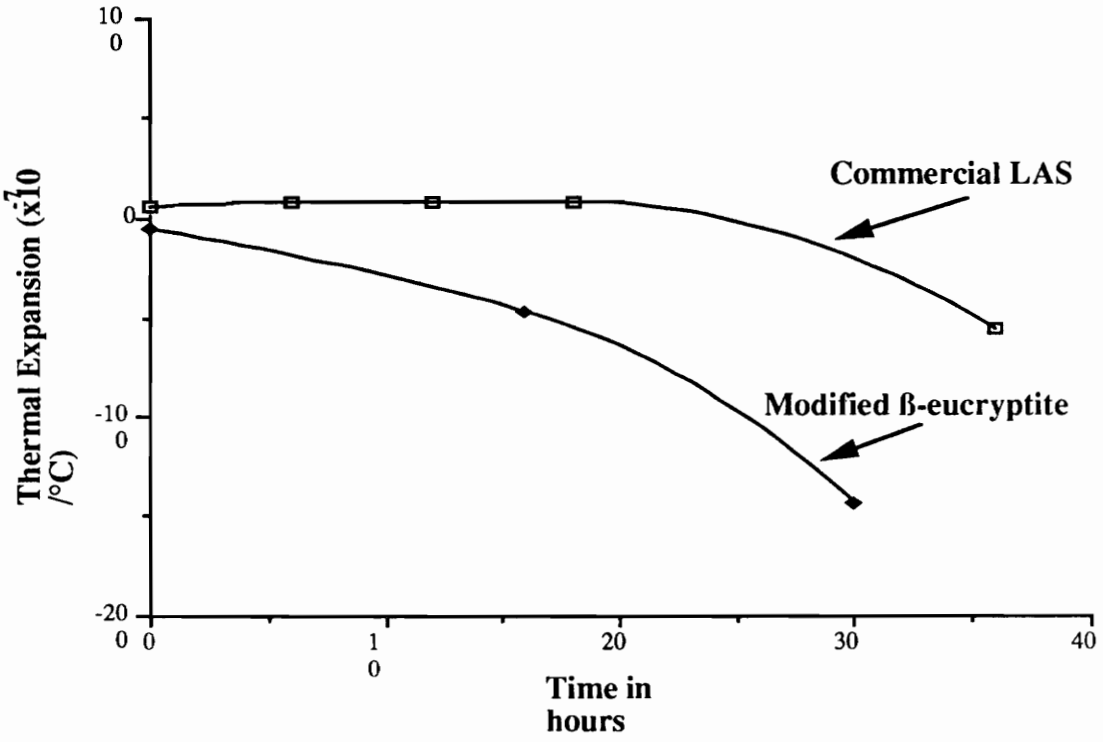

Figure 4.20: Thermal expansion coefficient of slip cast modified ß-eucryptite and commercial LAS after exposure to Na_2SO_4 at 1000°C

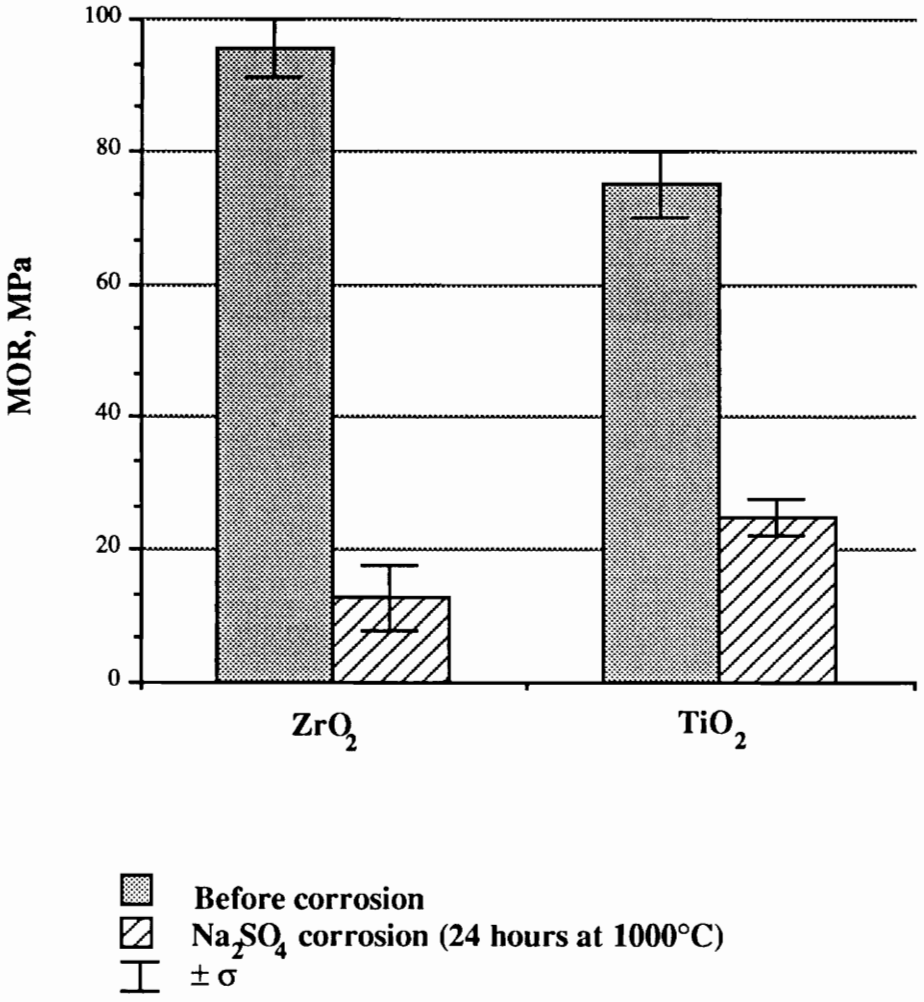

Figure 4.21: Modulus of rupture for modified ß-eucryptite (slip-cast (ZrO_2) and slip-cast TiO_2) samples).

the same order of magnitude for both of them: 78 percent of decrease for slip-cast (ZrO_2) and 73 percent for slip-cast (TiO_2) (Figure 4.22).

4.3.5 Summary

Slip-cast modified ß-eucryptite was corroded by Na_2SO_4 at high temperatures. Weight gain was observed due to the penetration of sodium and sulfur which formed an alkali melt under the sample surface. This led to large negative coefficients of thermal expansion, and a collapse of the mechanical properties. The decrease of the modulus of rupture was less important when TiO_2 was used as a nucleation agent because of the formation of TiO_2 fibers. The decrease of the Young's modulus was the same regardless the nucleation agent used.

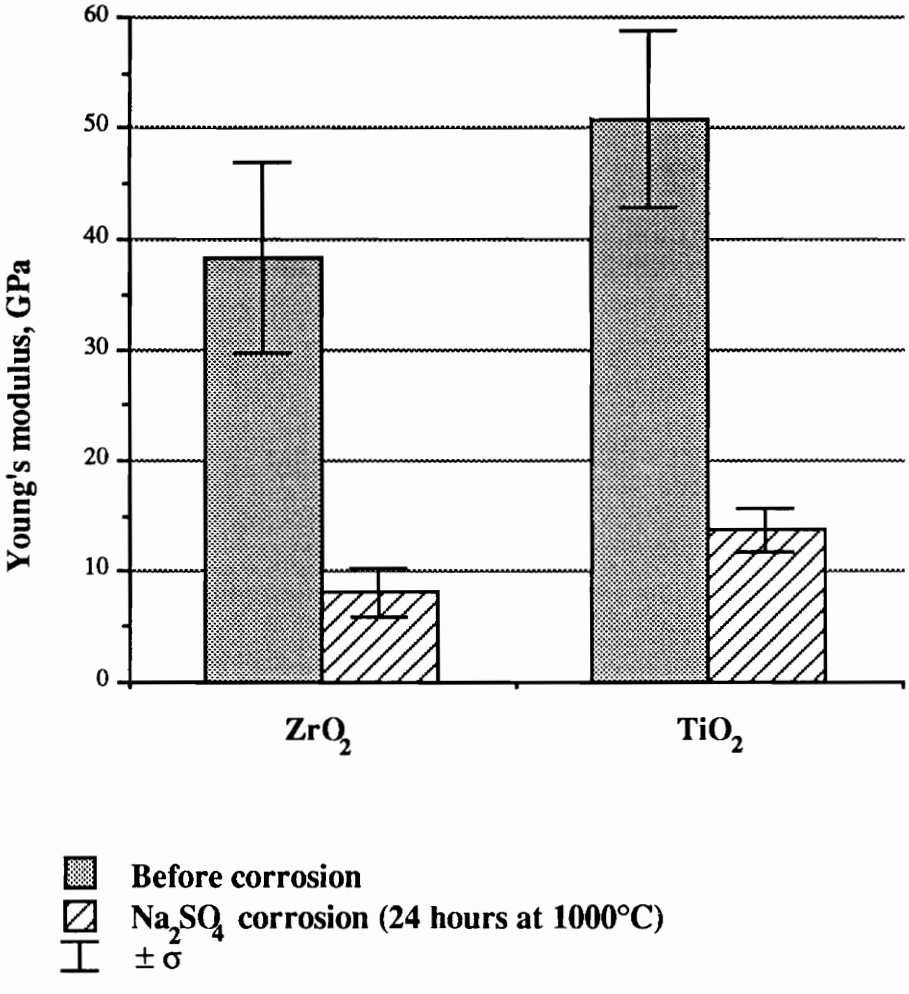

Figure 4.22: Young's Modulus for modified ß-eucryptite (slip-cast (ZrO_2) and slip-cast TiO_2) samples).

CHAPTER 5. CONCLUSIONS

1. Even though modified ß-eucryptite, $Li_{0.41}Mg_{0.035}AlP_{0.52}Si_{0.48}O_4$, has low expansion anisotropy and a near-zero coefficient of thermal expansion, it has a poor corrosion resistance to hydrochloric acid and molten sodium sulfate compared as to commercial LAS.

2. The poor corrosion resistance to HCl of modified ß-eucryptite is due to the removal of $AlPO_4$, which was used to decrease the anisotropy of ß-eucryptite.

3. The high temperature corrosion of slip-cast modified ß-eucryptite by Na_2SO_4 is caused by the penetration of sodium and sulfur which form an alkali melt under the sample surfaces.

4. Due to the removal of $AlPO_4$ in the case of HCl corrosion, the coefficient of thermal expansion decreases to more negative values towards the coefficient of thermal expansion

of pure ß-eucryptite. In the case of corrosion by Na_2SO_4, the formation of a melt under the sample surfaces led to large negative coefficient of thermal expansion.

5. Manufacturing processes which reduced the porosity and the formation of microcrack such as slip-casting, increased the corrosion resistance of modified ß-eucryptite to HCl and Na_2SO_4.

6. The modulus of rupture and the Young's modulus of slip-cast modified ß-eucryptite were reduced by HCl and Na_2SO_4; when TiO_2 was used as a nucleating agent instead of ZrO_2, the reduction of the modulus of rupture was less.

REFERENCES

1. C. A. Fucinari, "Regenerator Matrix - Physical Property Data", National Aeronautics and Space Administration, DOE/NASA/0008-80/11

2. W. Vogel, Chemistry of Glass, American Ceramic Society, Inc. (1985).

3. A. Paul, Chemistry of Glass, Chapman and Hall, New york (1982).

4. Z. Strinad, "Glass-ceramic Materials", Glass Science and Technology, vol 8.

5. Kingery, Bowen, Uhlmann, Introduction to Ceramics, second edition, John Wiley & Sons (1976).

6. V. Tscherry, H. Schulz, M. Czank, "Thermal Expansion of the Lattice Constants of ß-eucryptite Single Crystals, Ber. Deut. Keram. Ges., **49** (5) 153-4 (1972).

7. Y. Yang and J. J. Brown, "Thermal Expansion of Modified ß-eucryptite Compositions", presented at the 92nd Annual Meeting of American Ceramic Society (1990).

8. D. W. Richerson, Modern Ceramic Engineering, Properties, Processing, and Use, Manufactering Engineering and Materials Processing/8, Marcel Dekker, Inc., New York and Basel

9. L. A. Lay, Corrosion Resistance of Technical Ceramics, Her Majesty's Stationery Office, London (1983).

10. R. E. Swanson, "Galvanic Corrosion of Ceramics", Private communication.

11. J. R. Blachere, F. S. Pettit, High Temperature Corrosion of Ceramics, Noyes Data Corporation (1989).

12. D. S. Fox, N. J. Jacobson, J. L. Smialek, "Hot Corrosion of Silicon Carbide and Silicon Nitride at 1000°C", Ceramic Transactions, vol **10** (1990)

13. T. Sato, Y. Tokunaga, T. Endo, M. Shimada, K. Komeya, M. Komatsu, T. Kameda, "Corrosion of Silicon Nitride Ceramic in Aqueous Hydrogen Chloride Solutions", J. Am. Ceram. Soc., 71 [12] 1074-79 (1988).

14. J. E. Marra, E. R. Kreidler, N. S. Jacobson, D. S. Fox, "Reaction of Silicon-based Ceramics in Mixed Oxygen Chlorine Environments, J. Am. Ceram. Soc., **71** [12] 1067-73 (1988).

15. M. J. MacNallan, S. Y. Ip, S. Y. Lee, C. Park, "Corrosion of Silicon - based Ceramics in Mixed Oxygen Chlorine Environments, Ceramic Transactions, vol **10** 309-336 (1990).

16. N. S. Jacobson, J. L. Smialek, "Hot Corrosion of -SiC at 1000°C", J. Am. Ceram. Soc., **68** [8] 432-39 (1985).

17. N. S. Jacobson, "Kinetics and Mechanism of Corrosion of SiC by Molten Salts", J. Am. Ceram. Soc., **69** [1] 74-82 (1986).

18. J. L. Smialek, N. s. Jacobson, "Mechanism of Strength Degradation for Hot Corrosion of α-SiC", J. Am. Ceram. Soc., **69** [10] 741-52 (1986).

19. D. S. Fox, N. S. Jacobson, "Molten-Salt Corrosion of Silicon Nitride: I Sodium Carbonate", J. Am. Ceram. Soc., **71** [2] 128-38 (1988).

20. N. S. Jacobson, D. S. Fox, "Molten-Salt Corrosion of Silicon Nitride: II Sodium Sulfate", J. Am. Ceram. Soc., **71** [2] 139-48 (1988).

21. R. Bianco, N. S. Jacobson, "Corrosion of Cordierite Ceramics by Sodium Sulfate at 1000°C", Journal of Material Science, 2903-2910 (1989).

22. O. O. Van Der Biest, J. Barres, J. Corish, J. F. Norton, "Corrosion of a Silica-Bearing Ceramic in Sulfur Oxygen Atmospheres", J. Am. Ceram. Soc., **70** [7] 456-59 (1987).

23. H. Kim, A. Moorhead, "Effects of Active Oxidation on the Flexural Strength of -Silicon Carbide, J. Am. Ceram. Soc., **73** [7] 1868-72 (1990).

24. H. C. Cao, B. J. Dalgleish, C. H. Hsueh, A. G. Evans, "High-Temperature Corrosion Cracking in Ceramics", J. Am. Ceram. Soc., **70** [4] 257-64 (1987).

25. K. H. Lee, Private communications.

VITA

Laurent Battu was born on June 22, 1966 in France. He attended the Ecole Nationale Supérieure des Arts et Métiers in Paris and received his Engineering Diploma in June, 1989. After graduation, he entered the graduate program in Materials Engineering at Virginia Polytechnic Institute and State University